US Army Corps of Engineers

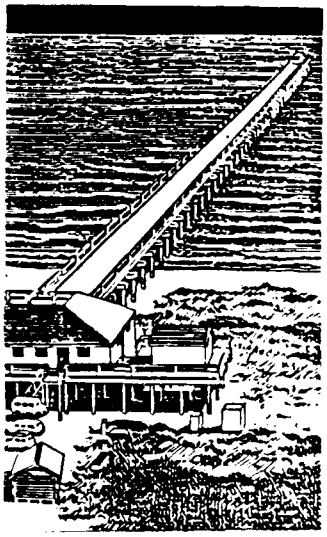

TECHNICAL REPORT CERC-88-11

(2)

UNIDIRECTIONAL SPECTRAL WAVE GENERATION AND ANALYSIS IN WAVE BASINS

Volume I

MAIN TEXT AND APPENDIX A

by

Michael J. Briggs

Coastal Engineering Research Center

DEPARTMENT OF THE ARMY
Waterways Experiment Station, Corps of Engineers
PO Box 631, Vicksburg, Mississippi 39181-0631

September 1988
Final Report

Destroy this report when no longer needed. Do not return it to the originator.

The findings in this report are not to be construed as an official Department of the Army position unless so designated by other authorized documents.

The contents of this report are not to be used for advertising, publication, or promotional purposes. Citation of trade names does not constitute an official endorsement or approval of the use of such commercial products.

Unclassified
SECURITY CLASSIFICATION OF THIS PAGE

AD-A199 749

REPORT DOCUMENTATION PAGE

Form Approved
OMB No 0704-0188
Exp Date Jun 30 1986

1a REPORT SECURITY CLASSIFICATION Unclassified	1b RESTRICTIVE MARKINGS
2a SECURITY CLASSIFICATION AUTHORITY	3 DISTRIBUTION / AVAILABILITY OF REPORT Approved for public release; distribution unlimited.
2b DECLASSIFICATION / DOWNGRADING SCHEDULE	
4 PERFORMING ORGANIZATION REPORT NUMBER(S) Technical Report CERC-88-11	5 MONITORING ORGANIZATION REPORT NUMBER(S)
6a NAME OF PERFORMING ORGANIZATION USAEWES, Coastal Engineering Research Center 6b OFFICE SYMBOL (If applicable)	7a NAME OF MONITORING ORGANIZATION
6c ADDRESS (City, State, and ZIP Code) PO Box 631 Vicksburg, MS 39181-0631	7b ADDRESS (City, State, and ZIP Code)
8a NAME OF FUNDING / SPONSORING ORGANIZATION US Army Corps of Engineers 8b OFFICE SYMBOL (If applicable)	9 PROCUREMENT INSTRUMENT IDENTIFICATION NUMBER
8c ADDRESS (City, State, and ZIP Code) Washington, DC 20314-1000	10 SOURCE OF FUNDING NUMBERS PROGRAM ELEMENT NO / PROJECT NO / TASK NO / WORK UNIT ACCESSION NO 31762

11 TITLE (Include Security Classification)
Unidirectional Spectral Wave Generation and Analysis in Wave Basins; Volume I: Main Text and Appendix A; Volume II: Appendixes B Through H

12 PERSONAL AUTHOR(S)
Briggs, Michael J.

13a TYPE OF REPORT	13b TIME COVERED	14 DATE OF REPORT (Year, Month, Day)	15 PAGE COUNT
Final report	FROM Jan 87 TO Aug 87	September 1988	245

16 SUPPLEMENTARY NOTATION
See reverse

17 COSATI CODES			18 SUBJECT TERMS (Continue on reverse if necessary and identify by block number)	
FIELD	GROUP	SUB-GROUP	Directional wave maker	Spectral waves
			Directional wave spectra	Wave calibration
			Physical models	Wave generation

19 ABSTRACT (Continue on reverse if necessary and identify by block number)

A series of 36 unidirectional spectral waves was generated to determine the relationship between wave generator control signal and measured response at seven locations in the model basin. Control signals consisted of combinations of three peak periods ranging from 1.0 to 2.0 sec, two zero-moment wave heights from 1 to 3 in., three spectral peak enhancement factors from 3.3 to 15, and two peak directions of 0 and -30 deg. Seven resistance or capacitance wave gages were centrally located 20 ft in front of the wave generator about its center line in a combination cross and 2-3-1-7 linear array. Descriptions of the spectral simulation and generation, time series and spectral analysis, frequency response, and wave grouping analysis are presented. Comparisons of predicted and measured peak period, zero-moment wave height, peak wave direction, frequency spectra, and directional spreading are presented and discussed. Frequency response and wave grouping statistics are calculated for each test case. This report consists of two volumes: Volume I consisting of the main text and Appendix A and Volume II consisting of Appendixes B-H.

20 DISTRIBUTION / AVAILABILITY OF ABSTRACT	21 ABSTRACT SECURITY CLASSIFICATION
☒ UNCLASSIFIED/UNLIMITED ☐ SAME AS RPT ☐ DTIC USERS	Unclassified
22a NAME OF RESPONSIBLE INDIVIDUAL	22b TELEPHONE (Include Area Code) / 22c OFFICE SYMBOL

DD FORM 1473, 84 MAR 83 APR edition may be used until exhausted
All other editions are obsolete

SECURITY CLASSIFICATION OF THIS PAGE

16. SUPPLEMENTARY NOTATION (Continued).

A limited number of copies of Volume II (Appendixes B Through H) was published under separate cover. Copies of Volume I (Main Text and Appendix A) are available from National Technical Information Service, 5285 Port Royal Road, Springfield, VA 22161.

PREFACE

This report is a product of the Laboratory Simulation of Spectral and Directional Spectral Waves Work Unit 31762, Coastal Flooding and Storm Protection Program, Civil Works Research and Development, US Army Corps of Engineers (USACE). Testing was conducted from January to April 1987, and data reduction and report preparation were completed in August 1987, at the US Army Engineer Waterways Experiment Station's (WES's) Coastal Engineering Research Center (CERC). Messrs. John H. Lockhart, Jr., and John G. Housley, USACE, were Technical Monitors for the Coastal Flooding and Storm Protection Program. Dr. C. Linwood Vincent was Program Manager at CERC.

This report was prepared by Mr. Michael J. Briggs, Research Hydraulic Engineer, under direct supervision of Mr. Douglas G. Outlaw, Chief, Wave Processes Branch, CERC, and under general supervision of Mr. C. E. Chatham, Chief, Wave Dynamics Division, Mr. Charles C. Calhoun, Jr., Assistant Chief, CERC, and Dr. James R. Houston, Chief, CERC.

Numerous individuals contributed to successful completion of this project, most notable of whom were Ms. Debbie L. Rouse, Computer Assistant, and Mr. Larry D. Davis, Contract Student. They assisted in every phase of the project, including simulating frequency spectra, generating control signals, calibrating wave gages, collecting and reducing data, and report preparation. Mr. David A. Dailey, Electronic Technician in the WES Instrumentation Services Division (ISD), maintained the directional spectral wave generator, wave gages, and associated electronics and obtained the wave gage calibrations. Mr. Barry W. McCleave, ISD Electronics Engineer, modified wave gage calibration and wave generation and measurement software. Mr. Larry A. Barnes, Civil Engineering Technician, provided expertise in design of support equipment and interfacing with the WES shops. Dr. Leon E. Borgman, University of Wyoming, developed the original directional wave simulation and analysis software and provided many hours of fruitful discussions. Finally, Mrs. Lee Ann Germany, Branch Secretary, assisted in preparation of the final report, and Mrs. Shirley Hanshaw of the WES Information Products Division edited this report.

Commander and Director of WES during publication of this report was COL Dwayne G. Lee, EN. Technical Director was Dr. Robert W. Whalin.

CONTENTS

---

* A limited number of copies of Appendixes B through H (Volume II) was published under separate cover. Copies are available from National Technical Information Service, 5285 Port Royal Road, Springfield, VA 22161.

CONVERSION FACTORS, NON-SI TO SI (METRIC)
UNITS OF MEASUREMENT

Non-SI units of measurement used in this report can be converted to SI (metric) units as follows:

Multiply	By	To Obtain
feet	0.3048	metres
horsepower (550 foot-pounds/sec)	745.6999	watts
inches	2.54	centimetres
pounds (mass)	0.4535924	kilograms
square feet	0.09290304	square metres

UNIDIRECTIONAL SPECTRAL WAVE GENERATION AND ANALYSIS IN WAVE BASINS

PART I: INTRODUCTION

Background and Purpose

1. The directional spectral wave generator (DSWG) at the US Army Engineer Waterways Experiment Station's (WES's) Coastal Engineering Research Center (CERC) provides a means to simulate real ocean environments in a laboratory physical model by incorporating directional spreading. Structures respond differently to spectral waves than they do to monochromatic waves. Thus, the transformation of wave energy in shallow and intermediate water depths due to shoaling, refraction, and diffraction on coastal structures such as harbors, breakwaters, jetties, mounds, artificial islands, and ship moorings can be studied.

2. Unidirectional spectral performance tests were conducted from January to April 1987. A series of 36 spectral waves was generated to determine the relationship between the DSWG control signal and the measured waves at seven different locations in the wave basin. The series consisted of combinations of three wave periods, two zero-moment wave heights, three spectral peakedness parameters, and two peak wave directions. Wave periods were 1, 1.5, and 2 sec, wave heights 1 and 3 in.,* peakedness parameters 3.3 and 7, and wave directions 0 and -30 deg. In addition, two tests with peakedness parameters of 15 were run at a peak wave direction of 0 deg to investigate the effect of spectral peakedness. Four tests were repeated to verify repeatability. Finally, four tests were run at a peak direction of 30 deg to note any differences in basin response due to wave orientation in the basin.

3. The purpose of this report is to present the unidirectional spectral wave test results. It deals with the mechanics of accurately simulating, generating, measuring, and analyzing unidirectional wave spectra. The verification of performance characteristics is a necessary first step in our overall research program before site-specific studies can be undertaken.

---

* A table of factors for converting non-SI units of measurement to SI

Report Organization

4. The report is divided into two volumes. Volume I contains the body of the report, presentation of results for a representative case, and an overall summary of results. Volume II is composed of appendixes which contain results for the rest of the cases.

5. A new method of generating unidirectional spectral waves has recently been implemented. In Part II, descriptions of this theory of simulation and generation of unidirectional spectral waves are presented. The generation program simulates a stroke time series for each of the 61 independent paddles of the DSWG using frequency domain methods and a "235" fast fourier transform (FFT) algorithm. Either deterministic amplitude and random phase (DSA) or random amplitude and phase (NSA) options are available. Two cases were run to compare these two simulation methods. The unidirectional wave spectrum is simulated as a product of a frequency spectrum and a directional spreading function. The desired frequency spectra may be an empirical TMA or Ochi-Hubble or discrete input at any selected frequencies. The directional spreading function may be an empirically derived wrapped normal or discrete input at equally spaced angles in a 360-deg circle. Although the directional spectrum may be multimodal in both frequency and direction space, only unimodal directional spectra were tested in this research effort. Also, only the TMA frequency spectrum and the wrapped normal spreading function were tested.

6. Part II also contains a description of the linear transfer function for directional "piston mode" wave makers for converting a wave elevation time series to corresponding strokes. These values are converted to digital voltage units prior to signal generation.

7. Part III describes the theory of time and frequency domain analyses of the measured data. Included are zero-downcrossing, spectral and unidirectional spectral, frequency response functions, and wave grouping. Three different methods of analysis are available for estimating the unidirectional spectral density estimates: (a) an eigenfunction procedure, (b) a method based on the Fourier series expansion of the directional spectrum, and (c) Maximum Liklihood Method (MLM). Only the second method is addressed in this report. The response amplitude operator (RAO) transfer functions are time domain equivalents of the ratios of the measured to predicted frequency

means of adjusting the control signals for more faithful reproduction of the desired spectral shapes. Finally, comparisons between Goda's and Kimura's methods are used to provide wave group statistics for a run of high waves from the measured data. Successive wave heights are assumed to be dependent, a fact which is observed in nature. Probability distributions and run lengths for both methods are described.

8. In Part IV, descriptions of the test setup, including the directional wave basin and generator, wave elevation measurement system, test case description, and test case generation and analysis parameters are given. One of the unique features of the DSWG is its flexible-plate seals between individual paddles which generate a more uniform wave form with less spurious waves. The directional wave basin is lined with wave absorber frames to minimize reflections. Resistance or capacitance wave gages with remote-controlled stepper motors were used. They were arranged in a 2-3-1-7 linear array incorporated in a cross pattern centrally located 20 ft in front of the DSWG about its center line. The unit lag spacing was designed to optimize resolution within the lower and upper cutoff frequencies while minimizing spatial aliasing.

9. Test results and analyses are presented in Part V. Time domain analysis results include time series traces of wave elevation and wave height for each test case. Frequency domain results include comparisons of predicted and measured peak wave periods, zero-moment wave height, peak wave direction, frequency spectra, and directional spreading function. A comparison of the DSA and NSA methods of unidirectional spectral generation is given. Also, RAO transfer functions as a function of frequency for each test case are presented. Wave group statistics for a run of high waves based on Goda's and Kimura's methods are presented next. Included are (a) the effect of lag length on the correlation coefficient, (b) probability distributions for run of high waves exceeding thresholds of the mean and significant wave heights, (c) effect of correlation coefficient on the mean run length for thresholds of mean and significant wave heights, (d) effect of correlation coefficient on the total run length, and (e) effect of Goda's peakedness parameter on the mean run length and the correlation coefficient.

10. Finally, Part VI contains a summary of results and recommenda-

wherever possible throughout this report and the computer software implemented for wave generation and analysis.

PART II: SPECTRAL SIMULATION AND GENERATION THEORY

Directional Wave Spectrum Parameterization

11. A directional or unidirectional wave spectrum $S(f,\theta)$* is usually parameterized as the product of two parts: a one-dimensional frequency spectrum $S(f)$ and a directional spreading function $D(f,\theta)$ as

$$S(f,\theta) = S(f)\, D(f,\theta) \tag{1}$$

where

f = frequency

θ = wave direction

The frequency spectrum and spreading function are subject to the following constraints:

$$S(f) = \int_0^{2\pi} S(f,\theta)\, d\theta$$

$$\int_0^{2\pi} D(f,\theta)\, d\theta = 1 \tag{2}$$

Frequency spectrum

12. The desired or target frequency spectrum may be input in one of three ways. It can be calculated according to the formula for an empirical TMA or Ochi-Hubble or input discretely from a numerical or field observation. Any number of frequencies can be used, and the spectrum can be multimodal (i.e. multiple peaks). For the research reported here, a unimodal, depth-limited TMA spectral form was used since it is most representative of intermediate to shallow-water wave conditions.

13. The TMA spectrum is a function of five parameters: peak frequency f_p, an alpha constant α, peak enhancement factor γ, spectral width parameter σ, and the water depth h. The first four parameters are those

associated with the Joint North Sea Wave Project (JONSWAP) spectrum. Vincent (1984) showed that the value for α can be estimated from the wave steepness ε such that it is valid for all water depths as follows:

$$\alpha = 16\pi^2 \varepsilon^2 \tag{3}$$

where

$\varepsilon = H_{m0}/(4 L_p)$

H_{m0} = zero-moment wave height = $4\sqrt{m_0}$

m_0 = area under the spectrum within lower and upper cutoff frequencies f_ℓ and f_u, respectively

L_p = wavelength associated with f_p

The peak enhancement factor controls the peakedness of the spectrum and typically varies between 1 to 3.3 for sea conditions to 7 and higher for swell waves. Both α and γ influence the energy contained in the wave spectrum. Typical values for the left σ_a and right σ_b spectral width parameters are 0.07 and 0.09, respectively. Like the JONSWAP spectrum, a wide range of single peaked spectra may be simulated by varying these five parameters. An expression for the TMA spectrum $S_{TMA}(f)$ in terms of the JONSWAP spectrum $S_J(f)$ is

$$S_{TMA}(f) = S_J(f) \times \Phi(f,h) \tag{4}$$

Kitaigorodskii et al. (1975) provides a full expression for Φ which can be approximated by

$$\Phi(f,h) = \begin{cases} \dfrac{\Omega_h^2}{2} & \text{for} \quad \Omega_h < 1 \\ 1.0 - \dfrac{(2 - \Omega_h)^2}{2} & \text{for} \quad 1 < \Omega_h < 2 \\ 1.0 & \text{for} \quad \Omega_h > 2 \end{cases} \tag{5}$$

where $\Omega = 2\pi f \times \sqrt{(h/g)}$.

Directional spreading function

14. The directional spreading function may be either an empirical wrapped normal (Borgman 1984) or input discretely at even increments within

360 deg. The wrapped normal spreading function was used in this study. It is a function of the principal direction θ_m and the spreading standard deviation σ_m. Both are linear functions of frequency f, consisting of a constant and slope component. The Fourier series representation for the wrapped normal spreading function is

$$D(F,\theta) = \frac{1}{2\pi} + \frac{1}{\pi} \sum_{\ell=1}^{L} \exp - \frac{(\ell\ \sigma_m)^2}{2} \cos \ell(\theta - \theta_m) \qquad (6)$$

where

$$\theta_m = \theta_0 + \theta_1 (f - f_p)$$
$$\sigma_m = \sigma_0 + \sigma_1 (f - f_p)$$

The number of harmonic terms L is arbitrarily selected to adequately represent the Fourier series of the directional spreading function. It can be of the order of 5 or as large as $6.0/\sigma_m$. In this study, both θ_1 and σ_1 were set to zero. For unidirectional spectral waves, a value of $\sigma_0 = 1$ is used.

15. One of the advantages of the wrapped normal spreading function is its high resolution. For a unidirectional spectrum, it has a large value at θ_m, representative of a Dirac delta function, and falls off rapidly for differences in angle, $\theta - \theta_m$, greater than 0 deg. After a 7-deg difference, the value of $D(f,\theta)$ is zero. Thus, care must be exercised in selecting the number of directional increments for simulating a unidirectional spreading function. For instance, for $\theta_m = 15$ deg and a directional increment of 22.5 deg, an erroneous value of $D(f,\theta) = 0$ at θ_m would be calculated. Therefore, a minimum of 36 increments at 10-deg intervals is necessary to ensure that the angular difference never exceeds 5 deg. In this study, 72 increments at 5 deg were used.

Wave Elevation Realizations

16. The psuedo-integral model (Borgman 1984, Briggs 1987c) for the unidirectional spectral surface elevation time series η at paddle location (x,y) and time t is

$$\eta(x,y,t) = 2 \int_0^{\infty} \int_0^{2\pi} A(f) \exp(-i\Phi) \exp(i\phi) \tag{7}$$

where

$A(f)$ = amplitude function described below

Φ = independent random phase, uniformly distributed on $(0,2\pi)$

$\phi = kx \cos\theta + ky \sin\theta - 2\pi ft$

k = wave number

θ = direction toward which waves travel, clockwise from x-axis

$i = \sqrt{-1}$

17. The model described by Equation 7 is a double summation model (Borgman 1969) since both frequency and direction are independent variables. Although this method is the preferred model to represent a directional sea, it is phase locked or phase dependent since different directions are summed at the same frequency. This phase locking gives a fluctuating RMS (i.e. root mean square) which tends to go to zero, however, as the number of components becomes large (Pinkster 1984). Thus, a long time series should be used. An alternate model to the double summation model is the single summation model. This model is sometimes preferred because less computer time and space are required and possible phase locking is not a concern. In this model, a single direction is randomly selected for each frequency component. A procedure for selecting this single direction (Sand and Mynett 1987) is to assign a cumulative directional distribution for each frequency and select a value using a uniform random distribution $U(0,1)$.

18. Realizations of the desired time series described in Equation 7 for the specified unidirectional wave spectrum are simulated in the frequency domain using one of two methods and then fourier transformed to the time domain. The first method is a deterministic amplitude, random phase only model (DSA) and the second method is a nondeterministic (Rayleigh) amplitude, random phase model (NSA) (Tucker, Challenor, and Carter 1984; Hudspeth, Nath, and Sollitt 1983; Isaacson 1985; Elgar, Guza, and Seymour 1984). Both methods also are known by other names including the Random Phase Method for the DSA method and the Random Coefficient Method for the NSA method (Sand and Mynett 1987).

19. In the DSA method, the fourier coefficients are calculated from the target spectrum with the deterministic amplitude A constrained to be

$$A(f) = \sqrt{[2\ S(f,\theta)\ df\ d\theta]} \tag{8}$$

They are then coupled with random phases and inverse fourier transformed using a "235" FFT to give the surface elevation time series. The length of the time series N is the product of the integers 2, 3, and 5 raised to integer powers, or

$$N = 2^K\ 3^L\ 5^M \tag{9}$$

In this method, the simulated spectrum always matches the target spectrum.

20. In the NSA method, Equation 7 is rewritten in an equivalent complex fourier series form. The complex amplitude A is defined by

$$A(f) = U(f) - i\ V(f) \tag{10}$$

where

$U(f)$ = real amplitude component

$V(f)$ = imaginary amplitude component

Both components are independent Rayleigh random variables with zero mean and variance $S(f,\theta)\ df\ d\theta$. These U and V components are obtained by first generating Gaussian distributed, zero mean, unit variance random variables which are then multiplied by the desired standard deviation (i.e. $\sqrt{[S(f,\theta)\ df\ d\theta)]}$. The inverse method of generating new random variables from a normal distribution is used to obtain the U and V components. If the normal or Gaussian probability function is defined

$$P(x) = u = \frac{1}{2\pi} \int_{-\infty}^{x} \exp\left(\frac{-t^2}{2}\right) dt \tag{11}$$

Then a new random variable x given by

$$x = P^{-1}(u) \tag{12}$$

can be generated using the approximation from Abramowitz and Stegun (1970)

$$c_0 + c_1 t + c_2 t^2$$

where

$$t = \sqrt{\ln\left(\frac{1}{u^2}\right)}$$

$c_0 = 2.515517$ $\quad$ $d_1 = 1.432788$

$c_1 = 0.802853$ $\quad$ $d_2 = 0.189269$

$c_2 = 0.010328$ $\quad$ $d_3 = 0.001308$

Again, an inverse FFT gives the simulated wave elevation time series. The NSA method differs from the DSA method in that the simulated spectral estimates do not exactly match the target spectrum but vary statistically about the true or desired spectral values. The variance of the variance is said to be more realistic than with the DSA method.

21. If there are many frequency and directional components in the wave train (i.e. of the order of 1,000 components), there is little difference between the DSA and NSA options for the complex wave amplitude. Both are asymptotically equivalent by the central limit theorem and behave very nearly as a Gaussian process in that case (Rice 1944, 1945; Elgar, Guza, and Seymour 1985). However, with some increase in computer time, the addition of the Rayleigh variable in the complex amplitude produces an exact Gaussian process. Addition of the Rayleigh variable is particularly useful for wave trains which are very narrow banded in both frequency and direction.

22. In summary, the least random (i.e. most deterministic) simulations involve the single summation model and the DSA method. The double summation model and NSA methods produce greater variance in the variance of the synthesized record. The procedure used in this study is predominantly the double summation model and the DSA method of frequency domain simulation.

Transfer Functions

23. Once the wave elevation time series have been simulated for each of the 61 DSWG paddles, they are converted to corresponding stroke time series using a height-to-stroke transfer function. The three-dimensional form F_3, which includes directional effects (Sand 1979), was originally derived by Biesel (1954) and is valid for all nondimensional water depths kh and is expressed as

Figure 1 illustrates how F_3 varies for frequencies between 0.1 to 2 Hz for the two wave directions of 0 and -30 deg used in this study. The wave breaking limit at the higher frequencies is also shown. This highest wave which can be generated at the wave maker (Ahrens 1986*) is

$$H_b = 0.1\ L \tanh kh \tag{15}$$

where L is wavelength.

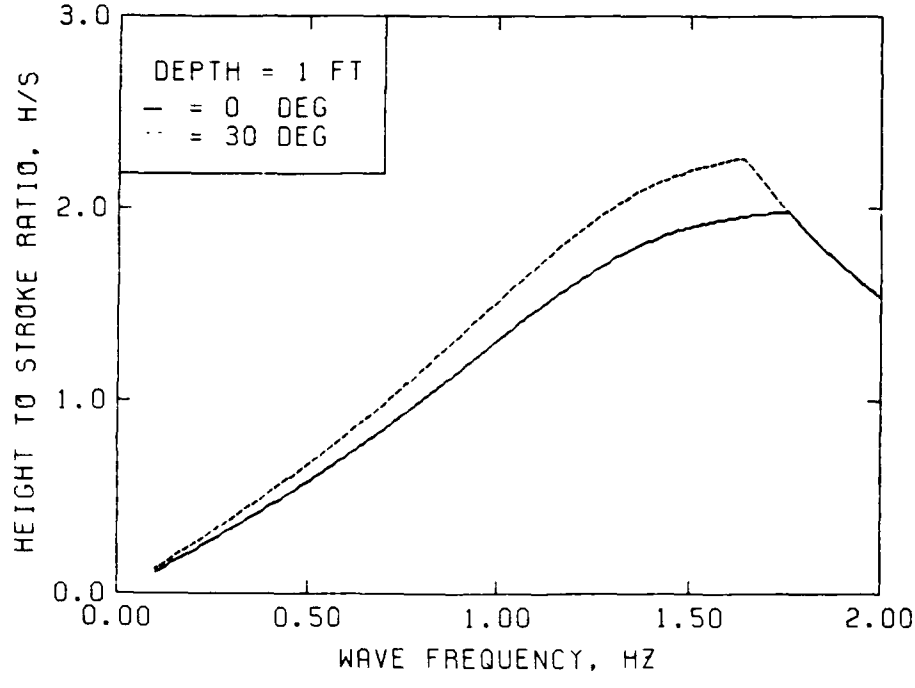

Figure 1. Height-to-stroke transfer function, including wave breaking limits

24. Finally, the stroke time-history is converted to a voltage time-history using the conversion factor for the wave maker. For the maximum stroke of 12 in., the DSWG has a peak-to-peak voltage of 20 v in 4,096 digital units. Thus, the conversion factor is 341.33 A/D units per inch or a resolution of 0.00293 in.

---

* Personal Communication, January 1986, John P. Ahrens, Research Oceanog-

PART III: TIME AND FREQUENCY DOMAIN ANALYSES

25. In all analyses, it is assumed that the wave elevation time series is a discrete, real-valued time sequence with equal time intervals $t = n\Delta t$. The relationship between the total length of the time series T_r and the total number of points N is $T_r = N\Delta t$. The value of N , although even, does not have to be a power of 2. The basic frequency increment is defined by $\Delta f = 1.0/T_r$.

Time Series Analysis

26. The time series analysis (TSA) package performs both time and frequency domain analyses of measured surface elevation data. Currently, the package allows 12 different processes to be run on the data. Time domain processes include time series strip charts of the raw data, zero upcrossing or downcrossing, crest and trough height, and autocorrelation and crosscorrelation. Frequency domain processes include autospectra or cross-spectra, frequency response between channels, coherence, and Goda reflection. Only three of the processes were used in this study: time series strip charts, zero downcrossing, and single channel spectral analysis. It is beyond the scope of this report to give a detailed description of the theoretical development of each process in the TSA. The interested reader is referred to the report by Long (in preparation) for more detailed descriptions of the algorithms.

27. The strip chart option plots the raw time series data for one or more of the available gages. The time series have not been detrended. The plots are cross-scaled to facilitate readability.

28. The zero downcrossing analysis calculates statistics of wave elevation, wave height, and period for the datum selected. This datum can be either the mean or an externally imposed value. For the surface elevation, the mean, root mean square, standard deviation, minimum, and maximum values are determined. Wave heights and periods corresponding to the difference between the minimum and maximum values between consecutive datum downcrossings are calculated. From these two arrays, mean and significant values are computed. Also, the total number of waves (i.e. zerocrossings) and the maximum wave height are given. Wave heights for each gage are saved for later plotting and use in the wave group analysis. Finally, cumulative probability

distributions and fitted Weibull distributions can be determined and plotted.

29. Spectral density estimates are calculated for individual gages after preprocessing to detrend and window the time series. Detrend options include removing the mean or a linear or second-order trend. Window options include 10 or 50 percent cosine bell or cubic polynomial. The data are fourier transformed, band averaged between lower and upper cutoff frequencies, and plotted. Measured spectral estimates for each gage are saved for later use in calculating frequency response estimates. Three different methods are used to calculate the peak frequency and corresponding period. The single line method gives the frequency having the largest energy content. The Delft method gives the mean frequency of all frequencies having energy content greater than or equal to 80 percent of the maximum. The CERC method gives the center frequency of the band of 11 consecutive frequencies having the largest total energy density. Zeroth, first, and second moments are estimated. Goda's (1970) peakedness parameter Q_p is also calculated. Finally, the average period from the zeroth and second moments is estimated.

Unidirectional Spectral Analysis

30. Three different methods for estimating $S(f,\theta)$ from an array of N surface wave gages are available. These are (a) an eigenfunction procedure, (b) a method based on the fourier series expansion of the directional spectrum, and (c) the MLM. Because of its simplicity, only the fourier method is used here.

Spectral formulation

31. The fourier series method is based on the relation (Borgman 1979, Briggs, Borgman, and Outlaw 1987) that the autospectra $S_{ii}(f)$ and cross-spectra $S_{ij}(f)$ between all pairs of wave elevation time series can be expressed as a linear combination of the directional components of $S(f,\theta)$ at that frequency. If the wave elevation time series n is defined as in Equation 7, then a system of equations for the spectral matrix of autospectra and cross-spectra in terms of $S(f,\theta)$ is

$$S_{ii}(f) = \int_0^{2\pi} S(f,\theta)\, d\theta \tag{16}$$

$$S_{ij}(f) = \int_0^{2\pi} S(f,\theta) \exp(iB_{ij})\, d\theta \qquad (17)$$

where

$B_{ij} = kX_{ij} \cos\theta + kY_{ij} \sin\theta$

$X_{ij} = x_i - x_j$

$Y_{ij} = y_i - y_j$

x = x-axis gage coordinates at location i or j

y = y-axis gage coordinates at location i or j

The cross-spectra are composed of real co-spectra C_{ij} and imaginary quadrature Q_{ij} components.

Parameterization of directional spectra

32. The first step toward solving the set of equations above is to parameterize $S(f,\theta)$ as the product of a frequency spectrum and a directional spreading function (Equation 1). The autospectral density $S_{ii}(f)$ for each of N gages is estimated, and then a combined best estimate $S(f)$ is obtained using a harmonic mean, as follows:

$$\bar{S}(f) = \left[\prod_{i=1}^{N} S_{ii}(f) \right]^{1/N} \qquad (18)$$

The directional spreading function is initially approximated by a truncated fourier series expansion of $L = 5$ harmonics.

$$D(f,\theta) = \frac{1}{2\pi} + \sum_{\ell=1}^{L} a_\ell(f) \cos(\ell\theta) + b_\ell(f) \sin(\ell\theta) \qquad (19)$$

where

$a_\ell(f)$ = real fourier coefficient of the spreading function

$b_\ell(f)$ = imaginary fourier coefficient of the spreading function

Spectral estimation of measured data

33. The next step is to calculate measured autospectral and cross-spectral density estimates for each gage and each gage pair, respectively. A

10 percent cosine bell window is applied in the time domain, and the cross-spectral matrix is calculated using the "235" FFT.

34. A Gaussian smoothing function is then used to smooth the estimates. This procedure is like "band averaging" since raw spectral estimates are smoothed in the frequency domain. However, it tends to give a smoother transition since it is more of a weighted moving average in that overlapping is used. The Gaussian smoothed line spectra $\bar{S}_m$ for each frequency $m\Delta f$ is defined as

$$\bar{S}_m = \frac{\sum_{j=-J}^{J} w_j S_{m-j}}{\sum_{j=-J}^{J} w_j} \tag{20}$$

where w_j is a weighting function defined below, and S_{m-j} is the raw auto-spectral or cross-spectral estimate at frequency $(m-j)\,\Delta f$. The weights are defined over an integer number of spectral lines J equivalent to $\pm 3\sigma$ standard deviations of a Gaussian curve, or

$$w_j = \exp\left[-\frac{(j\Delta t)^2}{2\sigma}\right] \tag{21}$$

Since the area under a Gaussian curve = $\sqrt{(2\pi)}\,\sigma$, an equivalent rectangle having the same area has height of 1.0 (at $x = 0$) and a bandwidth b defined by

$$\sigma = \frac{b}{\sqrt{(2\pi)}} \tag{22}$$

35. For Gaussian smoothing the number of bands averaged in each smoothed spectral estimate is considerably greater than a comparable frequency domain band averaging procedure. In band averaging, the resolution bandwidth b is the product of the number of bands averaged and the basic frequency increment Δf of the line spectra. In Gaussian smoothing the number of bands M in the smoothed average is given by

$$M = \frac{6\sigma}{\Delta f} \tag{23}$$

Solution procedure

36. The S_{ii} for each gage are inserted into the left-hand side of Equation 16. They are also substituted into Equation 18 to calculate S. The S_{ij} are calculated for each pair of gages and substituted into the left-hand side of Equation 17. The estimate for $\bar{S}$ and the parameterized directional spreading function $D(f,\theta)$ are substituted into the right-hand side of Equation 17 for $S(f,\theta)$. Thus, for N gages, a set of N^2 simultaneous linear equations (i.e. N autospectral equations of the form of Equation 16 and $N(N-1)/2$ pairs of cross-spectral equations of the form of Equation 17) can be solved for the fourier coefficients of the spreading function. However, since some of these equations may be theoretically zero, the number of available equations is usually less than N^2. The matrix form of this set of equations is

$$\{SPECTRA\} = [TRANSFER] * \{DIR\} \tag{24}$$

The vector {SPECTRA} consists of the measured S_{ij} estimates. The vector {DIR} is composed of the fourier coefficients for $D(f,i)$ at frequency f and is to be estimated. The matrix [TRANSFER] is therefore

$$[TRANSFER] = \int_0^{2\pi} \begin{bmatrix}\cos\\ \sin\end{bmatrix} (B_{ij}) \begin{bmatrix}\cos\\ \sin\end{bmatrix} (\ell\theta)\, d\theta \tag{25}$$

37. For an array of surface gages, Equation 25 could be expressed in the form of Bessel functions of order 1 (Borgman 1969, Borgman and Panicker 1970). Since the number of available equations (i.e. N^2) is greater than the number of unknown fourier coefficients (i.e. 10 for 5 harmonics), a least squares fourier transform method for numerical integration is used. The first step is inversion of the [TRANSFER] matrix to solve for the a_ℓ and b_ℓ spreading coefficients contained in the vector {DIR}. The technique for doing this is based on the vector linear regression model:

$$\{Y\} = [X] * \{B\} + \{\varepsilon\} \tag{26}$$

where

{Y} = n-component vector of dependent variables

[X] = n x k matrix of independent variables

{B} = k-component vector or regression coefficients

{ε} = n-component vector of prediction errors

The least square solution for {B} is given by the solution to the "normal equations"

$$\left([X]' * [X]\right) * \{B\} = [X]' * \{Y\} \tag{27}$$

where the prime denotes the matrix transpose. Principal components regression is used to invert Equation 24 based on the development of the Moore-Penrose generalized inverse from the eigenvector analysis of (X' * X) (Searle 1982).

38. The advantage of the Fourier method is its simplicity. The disadvantage is arbitrary truncation of the Fourier series at L (=5) harmonics where this number of coefficients (i.e. 2L + 1) is considerably less than the number of equations available. Stepwise regression tends to minimize this truncation effect. Jennrich (1977) specifies this least squares procedure which sequentially selects the "best" first harmonic coefficients. Next, "best" second harmonic coefficients are added, and another least squares iteration is performed with all coefficients. This procedure continues with "best" higher order harmonic coefficients being added one at a time until little improvement is realized after a least squares iteration.

39. The use of eigenvalue analysis helps to overcome the disastrous effects of an almost singular X'X matrix in Equation 27. It provides a number of eigenvalues which are significantly nonzero as an upper limit on the number of coefficients which can be estimated with the stepwise regression technique.

40. The $D(f,\theta)$ given in Equation 19 results in a distorted estimate of the true spreading function due to the truncation. This estimate is improved by fitting a parameterized wrapped normal formula (Equation 6) to the spreading function (Borgman 1979). Assuming that the lower order fourier coefficients are the least distorted by the truncation, they are used in the parameterized model to obtain estimates of the higher order coefficients. A new set of fourier coefficients (both lower and higher order) is calculated

using an iterative procedure until convergence is reached.

Principal direction
and directional spread

41. If the wrapped normal spreading function is defined as in Equation 6, the full-circle fourier coefficients a_ℓ and b_ℓ are

$$\begin{bmatrix} a_\ell(f) \\ b_\ell(f) \end{bmatrix} = \frac{1}{\pi} \int_0^{2\pi} D(f,\theta) \begin{bmatrix} \cos \\ \sin \end{bmatrix} (\ell\theta)\, d\theta \tag{28}$$

The corresponding coefficients for the first harmonic a_1 and b_1 are then

$$\begin{bmatrix} a_1(f) \\ b_1(f) \end{bmatrix} = \frac{1}{\pi} \begin{bmatrix} \cos \\ \sin \end{bmatrix} \theta_m \exp -\left(\frac{\sigma_m^2}{2}\right) \tag{29}$$

Therefore, the principal direction θ_m at frequency f is

$$\theta_m(f) = \arctan \left[\frac{b_1(f)}{a_1(f)}\right] \tag{30}$$

The mean of all θ_m equals $\bar{\theta}$.

42. Taking the magnitude of Equation 29 and rearranging gives the directional spread or standard deviation σ_m at frequency f, as follows:

$$\sigma_m(f) = \sqrt{-2 \ln \left\{\pi \sqrt{\left[a_1^2(f) + b_1^2(f)\right]}\right\}} \tag{31}$$

43. At each frequency, (N-1) independent estimates of each fourier coefficient are obtained. Various methods, including a weighted average or least squares, could be used to select a "best" choice. A simple average is used. A similar set of equations could be obtained for θ_m and σ_m if the second or higher order harmonic coefficients were used.

Response Amplitude Operator Function

44. The height-to-stroke transfer function discussed in Part II is

Because of leakage around and under a "wetback" wave maker, electronic and mechanical losses of the DSWG, use of linear wave theory, and basin response characteristics, the desired wave spectrum is usually not faithfully reproduced. Although the differences in spectral shape, peak period, and wave height may be slight, it is necessary to correct the control signal for accurate reproduction in future runs. This correction can be done once or iteratively over several runs until the improvement between corrections is slight. Thus, an RAO transfer function is calculated. Although the RAO was calculated for each case, it was not used in this study to correct the control signals.

45. The raw measured S_{ii} for each gage and predicted S_p spectral estimates are first Gaussian smoothed (see paragraph 34) to a desired bandwidth which must be equal to or greater than Δf . The RAO is then calculated in the frequency domain at each smoothed frequency as

$$RAO_i(f) = \sqrt{\left[\frac{S_{ii}(f)}{S_p(f)}\right]} \quad i = 1,2,3,\ldots N \tag{32}$$

An average of all points within each band or the midpoint in each band may be selected for each band. In addition to RAO's for individual gages, an average of all or a selected number of gages may be calculated. The RAO is set equal to 1.0 for those frequencies outside lower and upper cutoff frequencies (IAHR 1987) because of low signal-to-noise ratios. Also, RAO's greater than 10.0 or less than 0.1 are set to these respective upper and lower limits.

46. The stroke control signals s_c for each of the 61 paddles which produced the measured spectra are fourier transformed to the frequency domain for correction. The real and imaginary fourier coefficients U and V are divided at each frequency $m\Delta f$ by the appropriate value of the smoothed and averaged RAO. The RAO for an individual gage or an average of selected gages can be used. The fourier transform relationship is

$$U(m) - iV(m) = \Delta t \sum_{n=0}^{N-1} s_c(n\Delta t) \exp\left(\frac{-i2\pi mn}{N}\right) \tag{33}$$

The corrected fourier coefficients are then inverse fourier transformed to the time domain to give the new control signal

$$s_c(n\Delta t) = \Delta f \sum_{m=0}^{N-1} [U(m) - iV(m)] \exp\left(\frac{i2\pi mn}{N}\right) \qquad (34)$$

The square root in Equation 32 is necessary because spectral estimates are squared quantities of the fourier coefficients

$$S_{ii}(m) = \frac{1}{T_r} \left[U^2(m) + V^2(m)\right] \qquad i = 1,2,3,\ldots N \qquad (35)$$

The maximum crest and minimum trough digital values are 2,048 and -2,047, respectively. The digital control signals for the DSWG are low-pass filtered and converted to analog at run time.

Wave Grouping Analysis

47. High sea waves tend to fall into groups rather than appear individually. The coastal engineering research community has recognized the need to model wave groups as well as spectral waves. High waves in groups can produce more damage than isolated high waves. Engineers are finding that this grouping is important in the motions and resonances of moored structures and vessels, harbor resonance, stability and overtopping of shore protection structures, and surf beat. Because of the nature of wave grouping, its prediction, control, and analysis are especially important in shallow-water laboratory basins such as CERC's directional spectral wave basin.

48. A wave group is defined by the number of waves which exceed some arbitrary threshold, such as the mean or significant wave height. Figure 2 illustrates the concepts of a run of high waves and a total run. The length of the run of high waves is the number of waves above this threshold. The total run is the combination of the run of high waves followed by the run of low waves (i.e. succession of waves which fall below the threshold value). The total run is analogous to the zero-crossing period of the wave profile, except that the time series is composed of individual wave heights rather than surface elevations. Unless specified otherwise, it is assumed that a run of high waves is intended when a run length is mentioned.

49. This report presents the results from two different model fo-

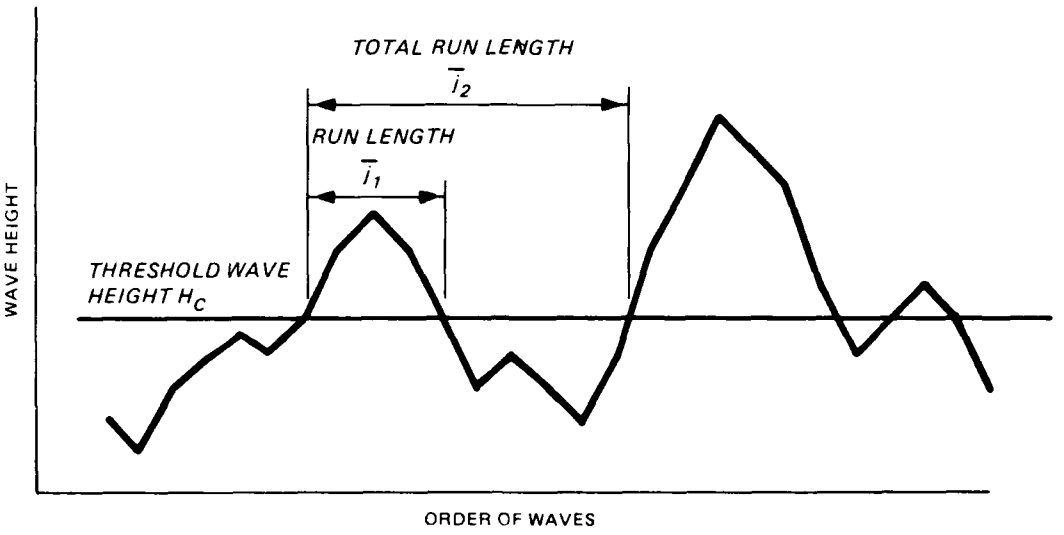

Figure 2. Wave grouping concepts

predicting wave group statistics from measured wave data in a laboratory basin. The first model is based on the work of Goda (1970). It assumes that successive wave heights are uncorrelated or independent, an appropriate assumption for broadband spectra. Goda's model is based on the Rayleigh distribution of wave heights, which assumes a narrow band spectrum. Thus, this model suffers from an internal inconsistency in that a wave field cannot be both broad and narrow banded. While Goda (1976) found good agreement for broad spectra and Elgar, Guza, and Seymour (1984) for spectra with $Q_p < 2$, Goda's model tends to break down for narrow spectra as the run length remains constant.

50. Kimura's model, on the other hand, assumes that successive wave heights are mutually correlated and form a Markov chain (Kimura 1980). The concept of mutual correlation implies that successive waves are dependent or correlated. Kimura's assumption is closer to what is observed in nature and has been found to better predict observed wave grouping due to sea and swell conditions than Goda's model (van Vledder 1983a,b; Thomas, Baba, and Harish 1986). Successive wave heights are indeed a dependent phenomenon. A high wave rarely appears by itself; it is more likely to be followed by other high waves. It is as though the waves have a "memory," which dictates that one high wave will be followed by another high wave rather than a low wave.

51. In the paragraphs below, descriptions of the probability distributions and run lengths for a run of high waves and a total run for both the

Goda and Kimura models are given. The interested reader is referred to a report and paper by Briggs (1987a,b) for more complete details.

Goda's model

52. If the probability p that a wave height H will be greater than a threshold value H_c is

$$p = \text{Prob}\,[H > H_c] \tag{36}$$

then the probability that this will not occur q is given by

$$q = \text{Prob}\,[H \leq H_c] = 1 - p \tag{37}$$

since $p + q = 1$. The probability distribution (Goda 1985) of a run of j_1 successive high waves $P(j_1)$ follows the geometric distribution

$$P(j_1) = p^{j_1-1}q \qquad j_1 = 1,2,3,\ldots \tag{38}$$

meaning that j_1-1 successive waves will exceed the threshold and the j_1^{th} wave will not. The probability of successive wave heights exceeding the threshold is equal to the product of separate probabilities for each event because the wave heights are independent. The mean run length of a run of high waves $\overline{j_1}$ is given by

$$\overline{j_1} = \frac{1}{q} \tag{39}$$

53. For a total run of j_2 successive waves, the probability distribution $P(j_2)$ and mean run length $\overline{j_2}$ are, respectively

$$P(j_2) = \frac{p\,q}{p - q}\left(p^{j_2-1} - q^{j_2-1}\right) \qquad j_2 = 1,2,3,\ldots \tag{40}$$

and

$$\overline{j_2} = \frac{1}{pq} \tag{41}$$

Kimura's model

54. A fundamental assumption of Kimura's model is that successive wave heights form a Markov chain. If a threshold wave height H_c is selected, waves with height H will fall into one of two states: state 1 where

$H \leq H_c$ or state 2 where $H > H_c$. A run of high waves begins when state 2 is first reached. A transition probability matrix [p] is given by

$$[p] = \begin{bmatrix} p_{11} & p_{12} \\ p_{21} & p_{22} \end{bmatrix} \tag{42}$$

where the individual elements are conditional probabilities. The first element p_{11} is the probability that neither successive wave exceeds the threshold H_c, and p_{22} is the probability of simultaneous exceedance by both wave heights.

55. These conditional probabilities p_{11} and p_{22} are defined in terms of the Rayleigh distribution. The Rayleigh probability density function (PDF) for individual wave heights, and the joint Rayleigh PDF for two successive wave heights are calculated numerically. The latter requires input of a correlation parameter κ which is related to the correlation coefficient R_{hh}, a measure of the degree of correlation or dependence between wave heights.

56. The correlation coefficient is calculated from the zero-meaned measured wave height time series. The autocorrelation function estimate is calculated and normalized by the variance to give the correlation coefficient

$$R_{hh}(k) = \frac{1}{\sigma^2} \frac{1}{N - k} \sum_{i=1}^{N-k} H_i \, H_{i+k} \qquad k = 1,2,3,... \tag{43}$$

where

N = total number of points in the wave height time series

σ = standard deviation of wave height time series

The lag k is the difference in number between wave heights and is equal to one for successive wave heights. For every other wave height, the correlation coefficient would be written as $R_{hh}(2)$, every third wave height $R_{hh}(3)$, etc. The dependency between wave heights has been found by several investigators (van Vledder 1983a, Arhan and Ezraty 1978, Goda 1983) to fall off rapidly as the lag is increased beyond successive wave heights (i.e., $R_{hh}(1)$).

57. The range of $R_{hh}(1)$ is 0 to 1.0. A value of zero corresponds to

the Goda model. Several investigators (Goda 1985; Thomas, Baba, and Harish 1986) have calculated correlation coefficients of 0.24 to 0.3 for successive wind waves and 0.5 to 0.8 for swell. The amount of correlation tends to increase with higher wave heights and narrower wave spectra.

58. Once $R_{hh}(1)$ is obtained from the measured data, κ is calculated using a series approximation proposed by Battjes (1974) and used in the transition probabilities p_{11} and p_{22}. This approximation is very good for correlation coefficients less than 0.7 to 0.8. From 0.8 to 1.0, the difference between the approximation and the exact value is slight.

59. Thus, for Kimura's model the probability of a run of successive high waves of run length j_1 is defined in terms of the transition probability p_{22} as

$$P(j_1) = p_{22}^{j_1-1} (1 - p_{22}) \qquad j_1 = 1,2,3,.... \tag{44}$$

The mean $\overline{j_1}$ is similarly defined as

$$\overline{j_1} = \frac{1}{1 - p_{22}} \tag{45}$$

Note the similarity of Equations 44 and 45 with Equations 38 and 39 for Goda's model: p_{22} and $(1 - p_{22})$ replace p and q, respectively.

60. For a total run of j_2 successive waves, the probability distribution $P(j_2)$ and mean run length $\overline{j_2}$ are, respectively,

$$P(j_2) = \frac{(1 - p_{11})(1 - p_{22})}{p_{11} - p_{22}} \left(p_{11}^{j_2-1} - p_{22}^{j_2-1} \right) \qquad j_2 = 1,2,3,... \tag{46}$$

$$\overline{j_2} = \frac{1}{1 - p_{11}} + \frac{1}{1 - p_{22}} \tag{47}$$

Again, note the similarity with the total run statistics defined for Goda's model in Equations 40 and 41.

PART IV: TEST SETUP

Wave Basin and Generator

61. Spectral waves were generated in CERC's 96-ft-long by 121-ft-wide directional spectral wave basin (Figure 3). It can accommodate water depths up to 2 ft. The bathymetry is uniform with maximum variations of 0.35 and 1.08 in. over a 5-ft distance and the entire basin, respectively (Briggs and Hampton 1987). The basin has a unique beach/wave absorption system, the perimeter of which is lined with wave absorber frames consisting of 2-in. layers of rubberized horsehair installed between two layers of expanded sheet metal. Each segment of the wave absorber beach opposite the wave generator is angled to deflect any reflected energy away from the primary measurement areas toward the sidewall absorbers (Figure 4). Flume tests by Briggs and Barnes (submitted) for a range of wave periods and heights demonstrated the effectiveness of the frame design. The average measured reflection coefficient of 12 percent is equivalent to a comparable gravel beach with a slope of 6 to 11 deg

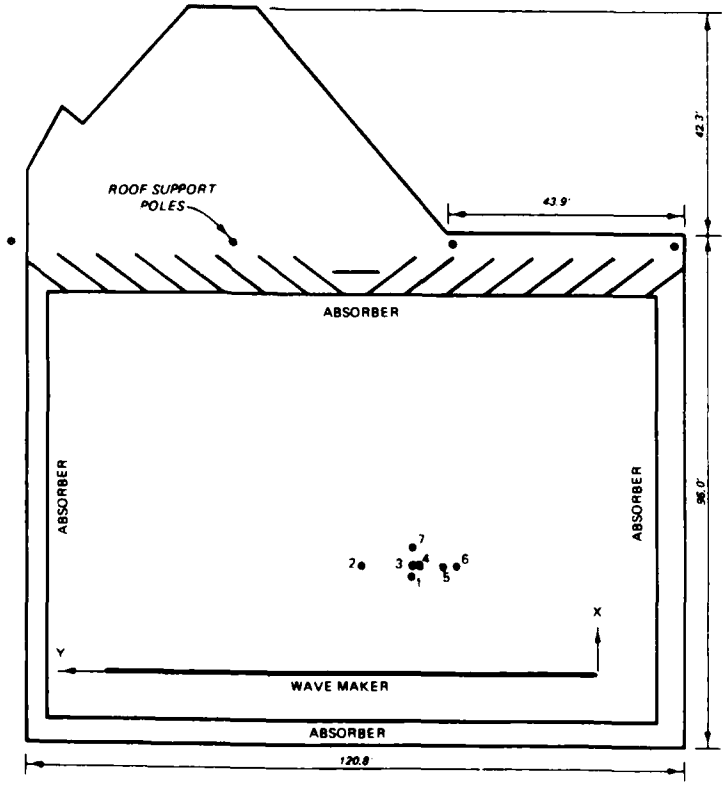

Figure 3. Schematic of basin and gage arrangement

Figure 4. Photograph of wave absorber frames along beach

which could be installed in the basin. Additional wave absorption is provided behind the beach segments by two rows (4 ft) of horsehair extending through the water column.

62. The DSWG was designed and constructed by MTS Systems Corporation, Minneapolis, Minnesota. It is 90 ft long and consists of 60 paddles in four modules of 15 paddles per module, each 1.5 ft wide and 2.5 ft high. It is an electronically controlled electromechanical system. The paddles are independently driven at each of the 61 joints in translational motion by a 0.75-hp electric motor. Each is connected with a flexible-plate seal to provide continuity and minimize the introduction of spurious waves (Outlaw and Briggs 1986).

63. The modular design allows one or more of the modules to be relocated to other physical model test sites to optimize usage. Because of this portability, it has no bottom or end seals and is referred to as a "wetback" design. During this test program only three of tne modules were used. Thus, the total length of the DSWG was 67.5 ft, and the center line was at Y = 33.75 ft.

Wave Elevation Measurement System

Gage description

64. Seven wave gages were used to measure surface wave elevations in the basin. Initially, parallel-wire resistance gages were used. Because these gages are sensitive to electronic and temperature drift and cleanliness of the water, they were replaced with capacitance gages. Flume and basin tests were conducted prior to this replacement to verify the accuracy of the capacitance gages.

Gage arrangement

65. The gages were mounted in aluminum frames to minimize inteference due to support legs and arranged in a directional array. Embedded in this array was a 2-3-1-7 linear array (Figure 3) patterned after the larger linear array design at CERC's Field Research Facility (FRF).* The linear array provides superior resolution capability for wave components at or near the same frequency and slightly different directions. This resolution can come about if the waves are directional or have been refracted.

66. A well-designed linear array must have a total length equal to the largest wavelength (i.e. lowest frequency) at the largest angle expected. It also must be short enough to avoid aliasing the higher frequency, smaller wavelength components. Spatial aliasing occurs when half the wavelength of the highest frequency wave does not exceed the distance between sensors. It is impossible to accurately discern the smaller wave from the longer wave. Thus, there is a classic tradeoff in that we want the longest array to optimize resolution of the low frequency components and the shortest spacing to minimize aliasing of the high frequency waves. The secret to this tradeoff is to select a minimum distance between two sensors which minimizes aliasing at the high frequency cutoff desired while simultaneously providing an overall length which optimizes resolution at the low frequency cutoff. By clever arrangement of a limited number of gages, both objectives can be achieved. Rather than spacing the gages a uniform distance apart, they are spaced at multiples of the unit lag length selected above. Thus, all wavelengths between the smallest and longest are covered by combinations of different gages.

---

* From handout at seminar, titled "Linear Arrays: Wind-Wave Directional Measurement Systems," presented by J. Oltman-Shay, March 1987, at the US

For the 2-3-1-7 array, wave periods with half wavelengths equal to 1, 2, 3, 4, 5, 6, 7, 8, 11, and 13 lags are discernible.

67. The procedure consists of calculating the depth-limited wavelength for the low and high frequency cutoffs desired. The y-axis wave number component k_y is calculated as

$$k_y = k \sin \theta \tag{48}$$

where $\theta > 0$ and a maximum wave direction to the linear array of $\theta = 30$ deg was assumed. The corresponding y-axis wavelength component L_y is then

$$L_y = \frac{2\pi}{k_y} \tag{49}$$

Finally, the array length capable of resolving this wavelength is equal to one-third to one-half of L_y. Based on this procedure, a lag spacing of 16 in. (1.33 ft) was selected for this study.

68. The two remaining gages were positioned in front of and behind the linear array for redundancy and possible reflection analysis. Table 1 summarizes the x- and y-axis coordinates of each of the seven gages in the directional array.

Table 1

Directional Array Coordinates

Gage No.	X-axis, ft	Y-axis, ft
1	18	33.75
2	20	43.08
3	20	33.75
4	20	32.42
5	20	28.42
6	20	25.75
7	23	33.75

Gage and depth calibration

69. The measurement rods on the gages had an overall length of 10 in. They were calibrated over a 6-in. range each day prior to conducting tests. A

Jordan controller stepper motor was used to automatically raise and lower the rod through a series of 11 steps to obtain calibration coefficients using a least squares linear or quadratic fit. This averaging technique, using 21 voltage samples per gage, minimizes the effects of slack in the gear drives and hysteresis in the sensors. Table 2 lists the quadratic fit and maximum deviation calibration coefficients (in units of feet times 10^{-5}) for each gage for each day of testing. The water depth was maintained within ±0.001 ft of the desired 1-ft level by an automatic water level float and solenoid control valve.

Table 2

Quadratic Fit Calibration Coefficients for Capacitance Wave Gages

Unidirectional Spectral Performance Tests

		Maximum Deviation, 10^{-5} ft									
		Gage No.									
No.	Date	RD01	RD02	RD03	RD04	RD05	RD06	RD07	Min	Max	Ave
1	3/5/87	314	355	79	123	390	150	367	79	390	254
2	3/11/87	81	249	75	143	97	123	274	75	274	149
3	4/9/87	← Not Available →									
4	4/17/87										
5	4/27/87	121	465	357	135	198	164	417	121	465	265
	Averages	172	356	170	134	228	146	353	92	376	223

Data Acquisition and Control System

70. An automated data acquisition and control system (ADACS) is used to create wave generator control signals for each of the 60 wave paddles, monitor wave paddle displacement feedback, and collect and analyze time series experimental data from the wave basin. The ADACS is controlled by a DEC VAX 11/750 central processing unit with capability for digital control signal output through an IEEE 488 interface and 120 channels of analog to digital input. The DSWG control signal is updated at a rate of 20 Hz. Additional information on the wave basin, wave generating system, and wave gages can be found in the report by Briggs and Hampton (1987).

Test Case Description

71. Thirty-four test cases, characterizing a range of unidirectional spectral parameters, were generated to quantify the performance characteristics of the DSWG. These cases consisted of combinations of three wave periods, two zero-moment wave heights, three spectral peakedness parameters, and two peak wave directions. Wave periods were 1, 1.5, and 2 sec, wave heights 1 and 3 in., peakedness parameters 3.3 and 7, and wave directions 0 and -30 deg. In addition, two tests with peakedness parameters of 15 were run at a peak wave direction of 0 deg to investigate the effect of spectral peakedness. Four tests with wave periods of 1.0 sec were repeated to verify repeatability. Finally, four tests at a wave period of 1.0 sec were run at a peak direction of 30 deg to quantify any differences in basin response due to wave orientation. Table 3 summarizes the spectral parameters for these 34 test cases.

Test Case Parameters

Simulation and generation phase

72. The D/A rate for the DSWG is 20 Hz (i.e. time increment of 0.05 sec), so 61 time series of 10,000 points or 500 sec were generated. This control signal duration corresponds to an even frequency increment of 0.002 Hz or 951 frequencies between the lower and upper cutoff frequencies of 0.1 to 2.0 Hz. The DSA amplitude procedure was used for control signal generation.

Data collection and analysis phases

73. After a waiting time of 25 sec to allow slower traveling high frequency components to travel beyond the farthest gage, wave elevation data were sampled at 10 Hz (i.e., time increment of 0.1 sec). A minimum of 200 waves at the peak period was collected as recommended by Goda (1985).

74. As recommended by IAHR (1986), zero downcrossing analysis was used to calculate time domain parameters. For spectral analysis, the data were zero meaned, tapered by a 10 percent cosine bell window, and band averaged within the lower and upper cutoff frequencies of 0.1 and 2.0 Hz, respectively. The resolution bandwidth is a function of peak wave period. Every 10 spectral lines were averaged to give 20 degrees of freedom. For the 1.0-sec peak period, the resolution bandwidth was 0.05 Hz. Table 4 lists the frequency

Table 3

Summary of Test Cases

Test Case ID	Period sec	Height in.	Alpha	Gamma	Angle deg	Gage Type*
			0-deg Series			
1	1.0	1	0.00332	3.3	0	R
2	1.0	1	0.00227	7.0	0	R
3	1.0	3	0.02990	3.3	0	R
4	1.0	3	0.02070	7.0	0	R
5	1.5	1	0.00113	3.3	0	R
6	1.5	1	0.00084	7.0	0	R
7	1.5	3	0.01030	3.3	0	R
8	1.5	3	0.00770	7.0	0	R
9	2.0	1	0.00059	3.3	0	R
10	2.0	1	0.00045	7.0	0	R
11	2.0	3	0.00538	3.3	0	R
12	2.0	3	0.00410	7.0	0	R
			-30 deg Series			
13	1.0	1	0.00332	3.3	-30	C
14	1.0	1	0.00227	7.0	-30	C
15	1.0	3	0.02990	3.3	-30	C
16	1.0	3	0.02070	7.0	-30	C
17	1.5	1	0.00113	3.3	-30	C
18	1.5	1	0.00084	7.0	-30	C
19	1.5	3	0.01030	3.3	-30	C
20	1.5	3	0.00770	7.0	-30	C
21	2.0	1	0.00059	3.3	-30	C
22	2.0	1	0.00045	7.0	-30	C
23	2.0	3	0.00538	3.3	-30	C
24	2.0	3	0.00410	7.0	-30	C
			Gamma 15 Series			
25	1.0	1	0.00144	15.0	0	C
26	1.0	3	0.01310	15.0	0	C
			Repeat Series			
27	1.0	1	0.00332	3.3	0	C
28	1.0	1	0.00227	7.0	0	C
29	1.0	3	0.02990	3.3	0	C
30	1.0	3	0.02070	7.0	0	C
			Orientation Series			
31	1.0	1	0.00332	3.3	30	R
32	1.0	1	0.00227	7.0	30	R
33	1.0	3	0.02990	3.3	30	R
34	1.0	3	0.02070	7.0	30	R

* R = resistance gage, C = capacitance gage.

Table 4

Collection and Analysis Parameters

Description	Peak Period, sec $T_p = 1$	$T_p = 1.5$	$T_p = 2$
Data Collection			
Record length, sec	200	300	400
No. points in record	2,000	3,000	4,000
Frequency increment, Hz	0.0050	0.0033	0.0025
Spectral Analysis			
Smoothed bandwidth, Hz	0.0500	0.0333	0.0250
No. frequency components analyzed	481	721	961
Unidirectional Spectral Analysis			
No. frequency components smoothed	23	35	47

dependent data collection and spectral analysis parameters for each of the three peak wave periods.

75. For the unidirectional spectral analysis, the data were again zero meaned, tapered by a 10 percent cosine bell window, and smoothed with a Gaussian smoothing function with an effective width of 0.05 Hz between the same lower and upper cutoff frequencies. Table 3 lists the number of frequencies Gaussian smoothed. All other parameters are the same as for spectral analysis. For the spreading function estimates, a resolution of 5 deg (i.e. 72 increments in 360 deg) was used. The predicted values were calculated without tapering the control signals.

PART V: TEST RESULTS AND ANALYSIS

Time Series Results

Time series plots

76. The measured wave elevation time series plot for gage 7, case 4 is shown in Figure 5. Gage 7 is representative of all gages. Plots for the other 33 cases are included in Appendix B (Volume II). The x-axis length is 200, 300, or 400 sec for peak period cases of 1.0, 1.5, and 2.0 sec, respectively. The y-axis scales have increments of 0.05 and 0.10 ft for wave height cases of 1 and 3 in., respectively. Comparisons among the 34 cases illustrate the effect of the period, height, spectral peakedness, and directional parameters.

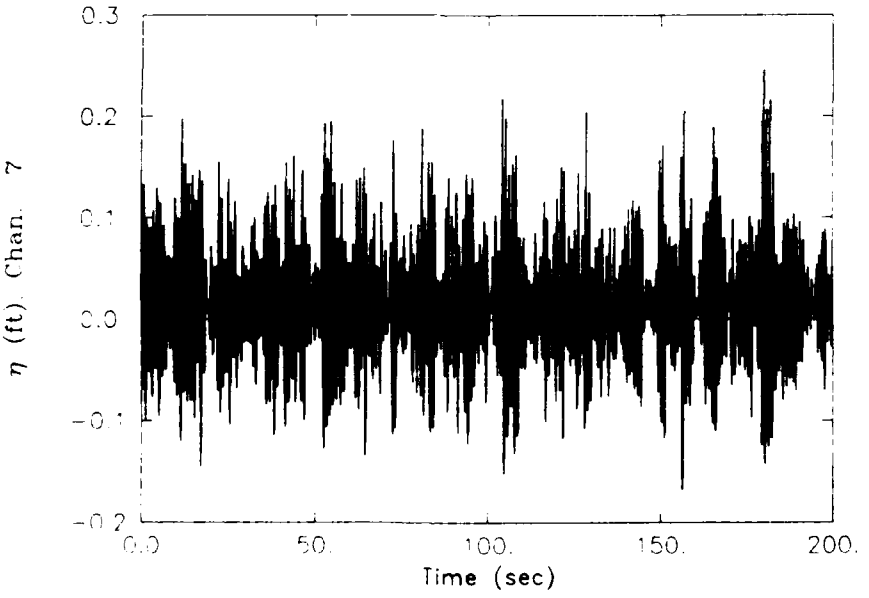

CASE 4, Tp=1.0, HmO=3, G=7.0, D=0

Figure 5. Measured wave elevation time series

Zero downcrossing

77. Results from the zero downcrossing analysis for each case are summarized in Table 5 which is organized like Table 3. The target wave period and height are listed for reference. The measured average values for all seven gages of the significant wave period $T_{H1/3,d}$ and significant wave height H [illegible] are given. A normalized value of each is listed in the last

Table 5

Zero Downcrossing Analysis Results

Test Case ID	Target Period sec	Target Height in.	Measured Average Period sec	Measured Average Height in.	Normalized Average Period	Normalized Average Height
			0-deg Series			
1	1.0	1.0	0.88	1.07	0.88	1.07
2	1.0	1.0	0.91	1.04	0.91	1.04
3	1.0	3.0	0.91	2.85	0.91	0.95
4	1.0	3.0	0.93	2.88	0.93	0.96
5	1.5	1.0	1.06	0.83	0.70	0.83
6	1.5	1.0	1.16	0.80	0.77	0.80
7	1.5	3.0	1.11	2.61	0.74	0.87
8	1.5	3.0	1.18	2.53	0.78	0.84
9	2.0	1.0	1.29	0.73	0.64	0.73
10	2.0	1.0	1.44	0.70	0.72	0.70
11	2.0	3.0	1.31	2.37	0.65	0.78
12	2.0	3.0	1.44	2.30	0.72	0.78
			-30 deg Series			
13	1.0	1.0	0.93	0.82	0.93	0.82
14	1.0	1.0	0.94	0.84	0.94	0.84
15	1.0	3.0	0.93	2.60	0.93	0.87
16	1.0	3.0	0.96	2.70	0.96	0.90
17	1.5	1.0	1.21	0.62	0.81	0.62
18	1.5	1.0	1.34	0.67	0.89	0.67
19	1.5	3.0	1.28	2.21	0.85	0.74
20	1.5	3.0	1.34	2.23	0.89	0.75
21	2.0	1.0	1.57	0.61	0.78	0.61
22	2.0	1.0	1.70	0.60	0.85	0.60
23	2.0	3.0	1.59	2.03	0.79	0.68
24	2.0	3.0	1.72	2.06	0.86	0.68
			Gamma 15 Series			
25	1.0	1.0	0.93	0.98	0.93	0.98
26	1.0	3.0	0.94	2.89	0.94	0.96
			Repeat Series			
27	1.0	1.0	0.86	1.03	0.86	1.03
28	1.0	1.0	0.90	1.02	0.90	1.02
29	1.0	3.0	0.91	2.83	0.91	0.94
30	1.0	3.0	0.94	2.95	0.94	0.98
			Orientation Series			
31	1.0	1.0	0.90	0.83	0.90	0.83
32	1.0	1.0	0.93	0.84	0.93	0.84
33	1.0	3.0	0.91	2.43	0.94	0.81
34	1.0	3.0	0.94	2.50	0.91	0.83

two columns. It is the ratio of the measured period or height normalized by the target value. Appendix C lists all TSA results for each of the seven gages.

78. Measured average periods are plotted against target period for 0-deg (i.e. 1-12 and 25-26) and -30 deg (i.e. 13-24) cases in Figures 6a and 6b, respectively. The cases are grouped by spectral peakedness. Normalized values for wave period ranged from a low of 0.64 for case 9 at 2.0 sec and 0 deg to a high of 0.96 for case 16 at 1.0 sec and -30 deg. The measured periods for the eight 0-deg cases at larger periods of 1.5 and 2.0 sec seemed to be much lower than their target values, especially relative to the -30 deg series cases. The normalized period values for these eight cases were 0.11 to 0.14 lower than their counterparts in the -30 deg series. Disregarding these eight cases, the lowest normalized period was 0.78.

79. Measured average wave heights are shown in Figures 7a and 7b for the 0-deg and -30 deg series cases, respectively. Again, they are grouped by gamma. The two wave height levels are shown individually. As previously observed for the monochromatic waves (Briggs and Hampton 1987), wave height decreased as period and wave direction increased. The normalized wave heights ranged from a low of 0.60 for case 22 at 2.0 sec and -30 deg and a high of 1.07 for case 1 at 1.0 sec and 0 deg.

80. Results from the repeatability tests are shown in Figure 8. It shows the measured average wave heights for cases 1-4 (x-axis) plotted against the corresponding cases 27-30 (y-axis). The agreement is excellent. Figure 9 illustrates the effect of wave orientation on the measured wave height for cases 13-16 at -30 deg (x-axis) versus cases 31-34 at 30 deg (the y-axis). The agreement is very good with a slight variation for the 3-in. waves. Finally, the agreement is excellent between measured wave periods for both sets of cases.

Spectral analysis

81. Spectral analysis results include calculation of spectral statistics and frequency spectra plots. These statistics include peak wave period T_p , zero-moment wave height H_{m0} , and Goda peakedness parameter Q_p .

82. Spectral statistics. Table 6 lists statistics for the spectral analysis of each of the 34 cases. Again, the test case numbers and target wave period and height are given for reference. The measured average of all seven gages for T_p and H_{m0} are listed. The normalized values are

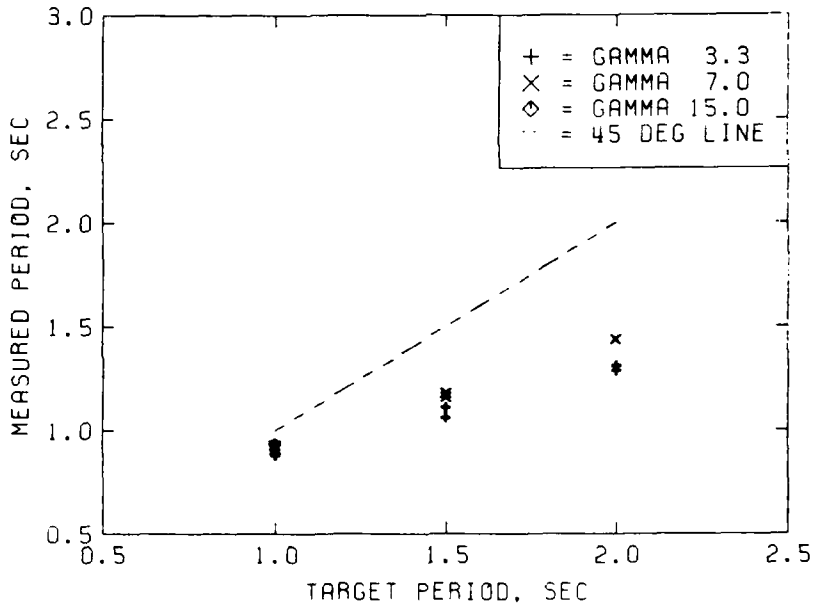

14 DOWNCROSSING CASES: CASES 1-12 & 25-26

a. Cases of 0 deg

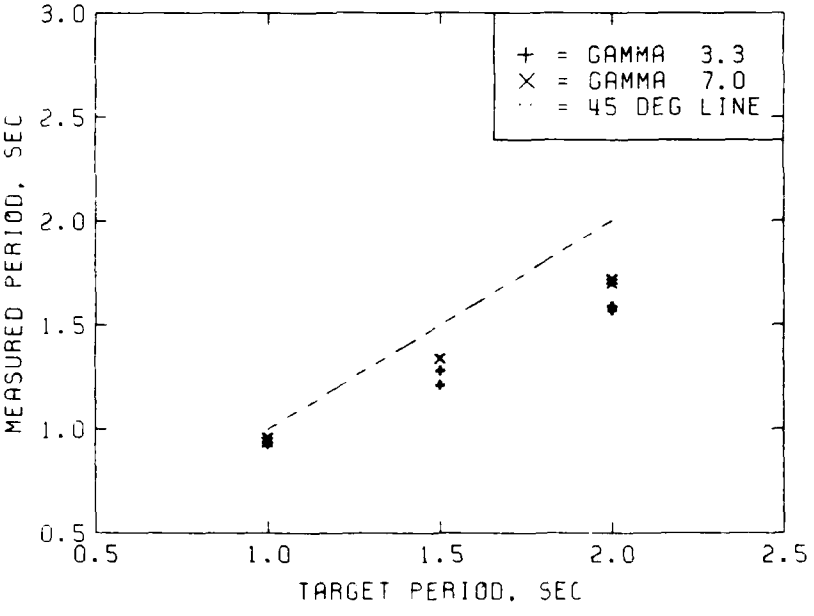

12 DOWNCROSSING CASES: CASES 13-24

b. Cases of -30 deg

Figure 6. Measured versus target zero-crossing wave periods

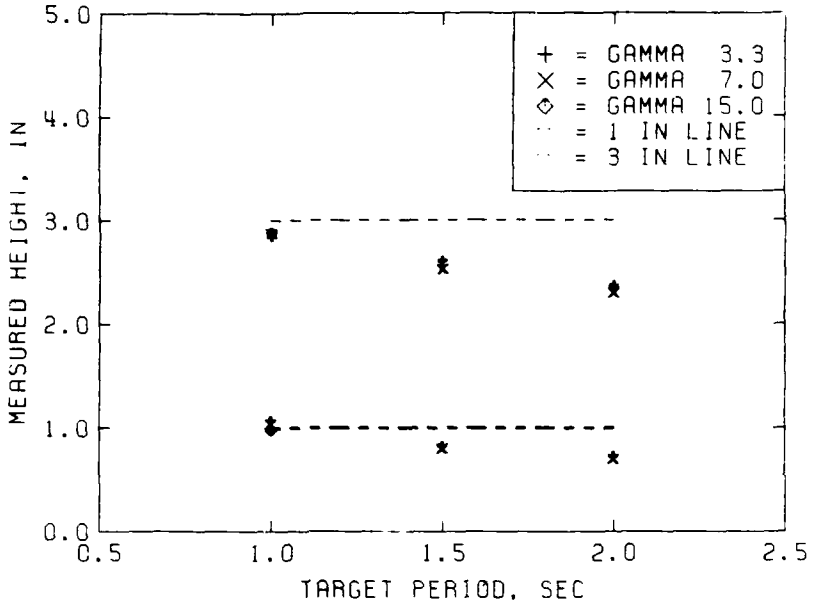

14 DOWNCROSSING CASES: CASES 1-12 & 25-26

a. Cases of 0 deg

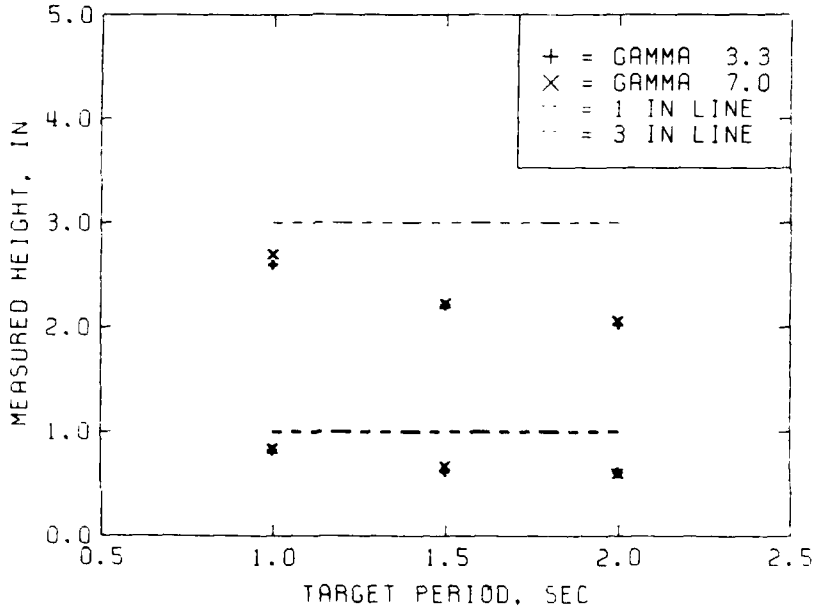

12 DOWNCROSSING CASES: CASES 13-24

b. Cases of -30 deg

Figure 7. Measured versus target zero-crossing wave heights

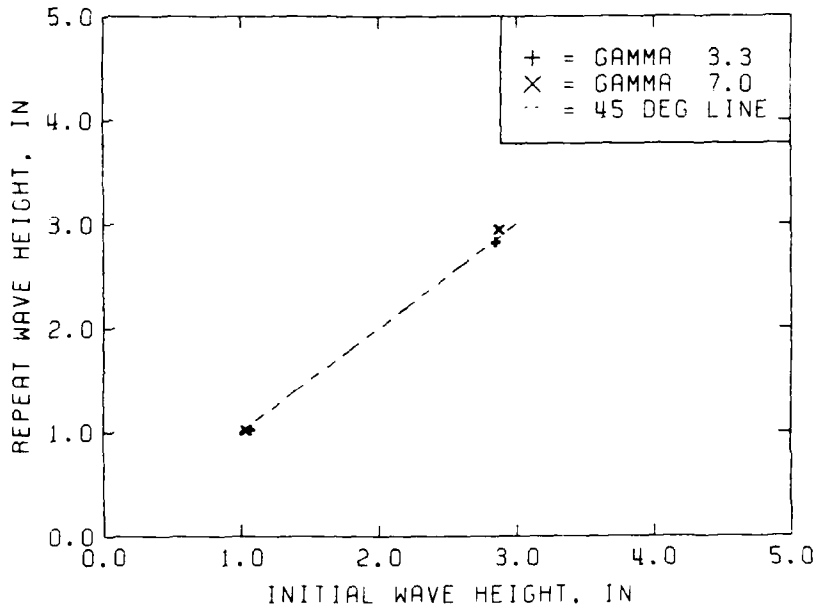

4 DOWNCROSSING CASES: CASES 1-4 VS. 27-30

Figure 8. Repeatability series of zero-crossing wave heights

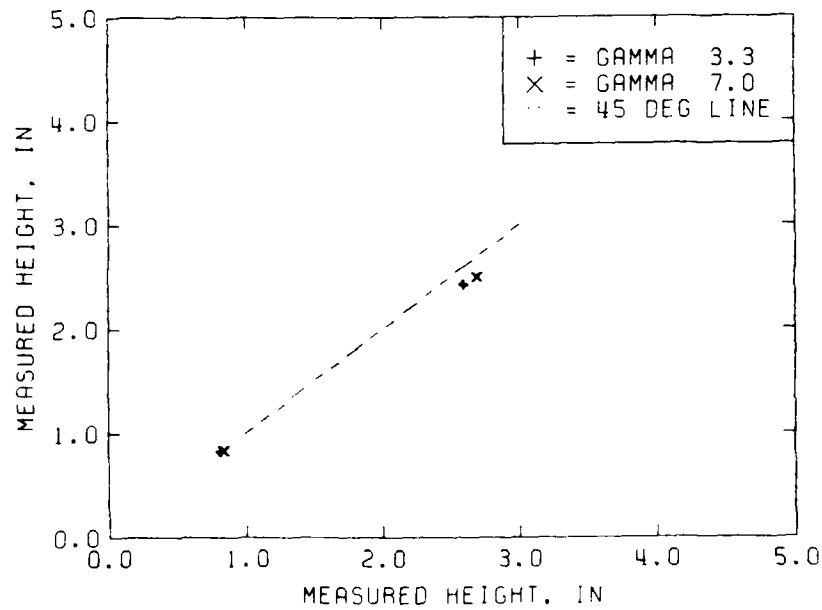

4 DOWNCROSSING CASES: CASES 13-16 VS. 31-34

Figure 9. Orientation series of zero-crossing wave heights

Table 6

Spectral Analysis Results

Test Case ID	Target Period sec	Target Height in.	Measured Average Period sec	Measured Average Height in.	Normalized Average Period	Normalized Average Height	Goda Spectral Peakedness
			0-deg Series				
1	1.0	1.0	0.97	1.15	0.97	1.15	3.18
2	1.0	1.0	0.99	1.11	0.99	1.11	4.11
3	1.0	3.0	1.01	2.93	1.01	0.98	3.24
4	1.0	3.0	1.02	2.96	1.02	0.99	4.23
5	1.5	1.0	1.44	0.90	0.96	0.90	1.87
6	1.5	1.0	1.51	0.87	1.01	0.87	2.28
7	1.5	3.0	1.40	2.76	0.94	0.92	1.85
8	1.5	3.0	1.44	2.68	0.96	0.89	2.13
9	2.0	1.0	1.92	0.80	0.96	0.80	1.63
10	2.0	1.0	1.92	0.77	0.96	0.77	2.20
11	2.0	3.0	1.97	2.54	0.99	0.85	1.54
12	2.0	3.0	1.97	2.48	0.99	0.83	2.04
			-30 deg Series				
13	1.0	1.0	1.00	0.86	1.00	0.86	4.37
14	1.0	1.0	0.99	0.89	0.99	0.89	5.83
15	1.0	3.0	0.98	2.67	0.98	0.89	4.09
16	1.0	3.0	1.02	2.75	1.02	0.92	5.38
17	1.5	1.0	1.46	0.66	0.97	0.66	2.34
18	1.5	1.0	1.51	0.72	1.01	0.72	3.49
19	1.5	3.0	1.49	2.32	0.99	0.77	2.40
20	1.5	3.0	1.52	2.35	1.01	0.78	3.14
21	2.0	1.0	1.94	0.65	0.97	0.65	2.21
22	2.0	1.0	1.94	0.64	0.97	0.64	3.13
23	2.0	3.0	1.96	2.16	0.98	0.72	2.17
24	2.0	3.0	1.98	2.18	0.99	0.73	3.19
			Gamma 15 Series				
25	1.0	1.0	0.98	1.06	0.98	1.06	6.59
26	1.0	3.0	1.01	2.96	1.01	0.99	5.92
			Repeat Series				
27	1.0	1.0	1.00	1.11	1.00	1.11	3.00
28	1.0	1.0	0.99	1.09	0.99	1.09	3.88
29	1.0	3.0	0.99	2.89	0.99	0.96	3.32
30	1.0	3.0	1.02	3.01	1.02	1.00	4.41
			Orientation Series				
31	1.0	1.0	1.00	0.88	1.00	0.88	4.06
32	1.0	1.0	0.99	0.90	0.99	0.90	6.11
33	1.0	3.0	1.00	2.51	1.00	0.84	3.76
34	1.0	3.0	1.01	2.55	1.01	0.85	5.45

calculated as before. Goda's Q_p is listed in the last column for use in the wave grouping analysis.

83. Measured average periods are plotted against target periods for 0-deg (i.e. 1-12 and 25-26) and -30 deg (i.e. 13-24) cases in Figures 10a and 10b, respectively. They are analogous to Figures 6a and 6b. The range of normalized periods is from a low of 0.94 for case 7 at 1.5 sec and 0 deg to a high of 1.02 for cases 4, 16, and 30 at 1.0 sec. This variation in measured periods is much less than the corresponding zero-crossing values.

84. Measured average wave heights are shown for the 0-deg and -30 deg series cases in Figures 11a and 11b, respectively. They are analogous to Figures 7a and 7b for the zero-crossing analysis. The cases are grouped by gamma and wave height. The normalized heights varied from a low of 0.64 for case 22 at 2.0 sec and -30 deg to a high of 1.15 for case 1 at 1.0 sec and 0 deg. Again, wave height decreases with increasing wave period and direction. Even though these values differed in period and height from their target values, they are much closer than the corresponding zero-crossing analysis results. The RAO transfer functions should correct the control signals to give the required wave heights.

85. Figures 12 and 13 show the repeatability and wave orientation test series wave heights, respectively. The format is the same as for Figures 8 and 9 for the zero-crossing analysis. The variations in wave period and height for the repeat and wave orientation series with their counterparts were insignificant.

86. Frequency spectra. Figure 14 illustrates the measured versus predicted frequency spectra for case 4: T_p = 1.0 sec, H_{m0} = 3 in., γ = 7.0 , and D = 0 deg. This case is used throughout this report as an example. Plots of the other cases are included in Appendix D. The x-axis is from 0 to 2.0 Hz. The y-axis varies according to wave height. The range is 0 to 3 for 1-in. waves and 0 to 24 for 3-in. waves. The dashed line is the predicted spectrum and the solid line gives the measured spectrum. The agreement is excellent.

87. The agreement for the 1.0-sec cases was generally excellent for all cases regardless of wave height, direction, or spectral peakedness. The shape of the spectra for the longer period cases was not as accurate as desired. The measured spectral peak in these cases was usually less than the predicted value by a factor of the order of 2. The magnitude of the low frequency tail

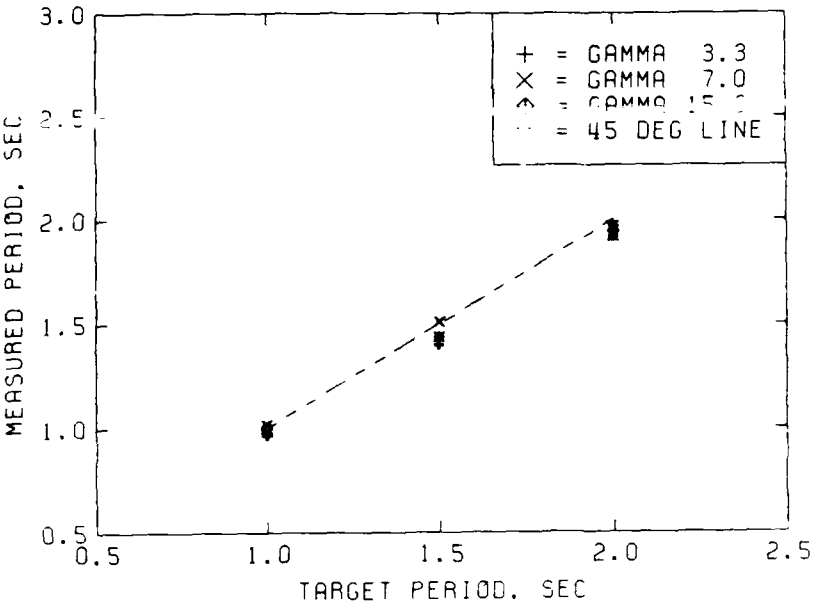

14 SPECTRAL CASES: CASES 1-12 & 25-26

a. Cases of 0 deg

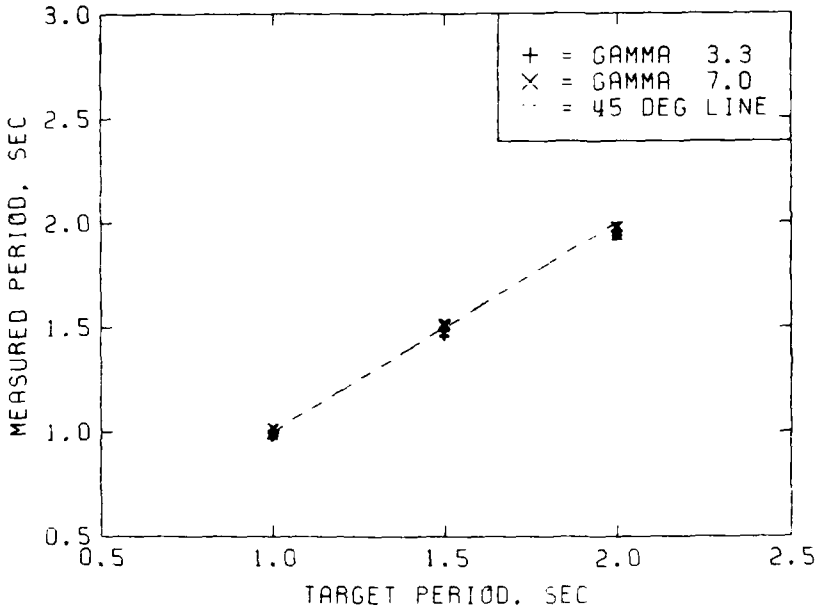

12 SPECTRAL CASES: CASES 13-24

b. Cases of -30 deg

Figure 10. Measured versus target spectral wave periods

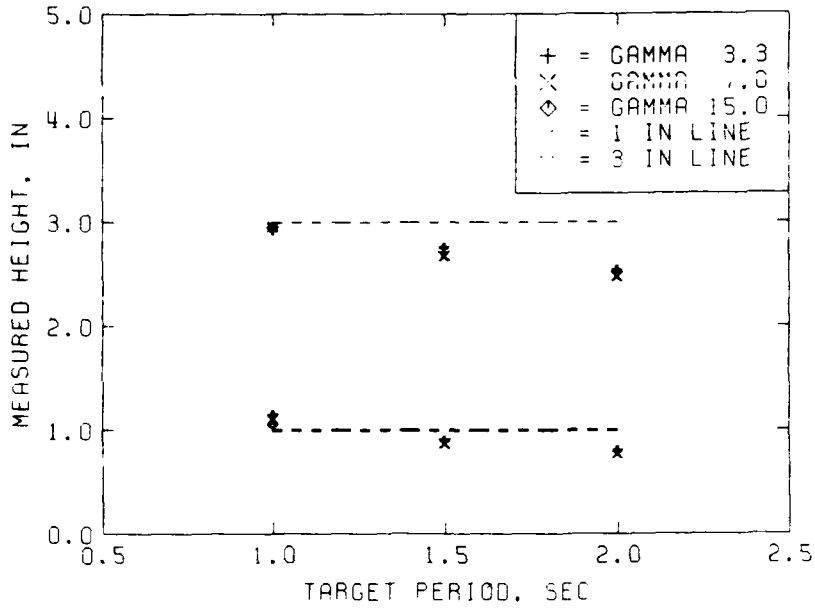

14 SPECTRAL CASES: CASES 1-12 & 25-26

a. Cases of 0 deg

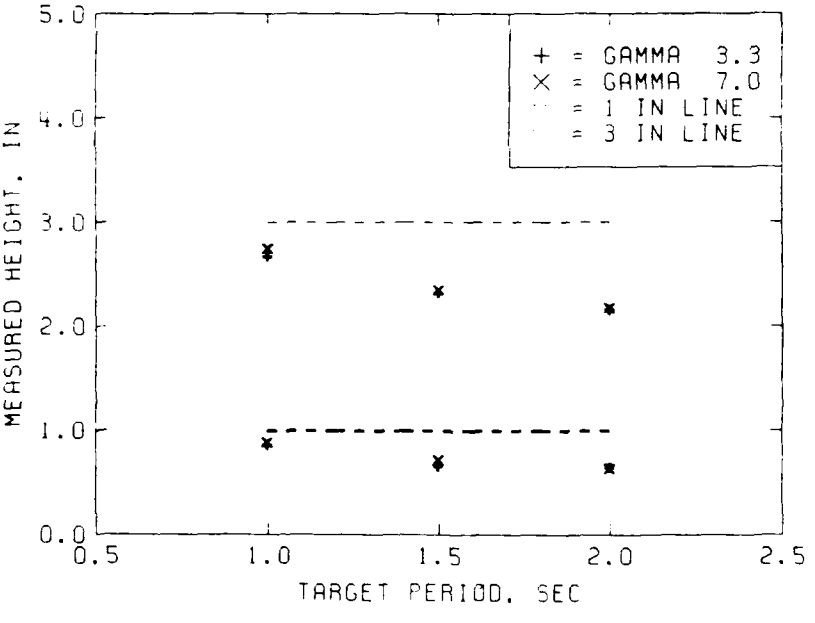

12 SPECTRAL CASES: CASES 13-24

b. Cases of -30 deg

Figure 11. Measured versus target spectral wave heights

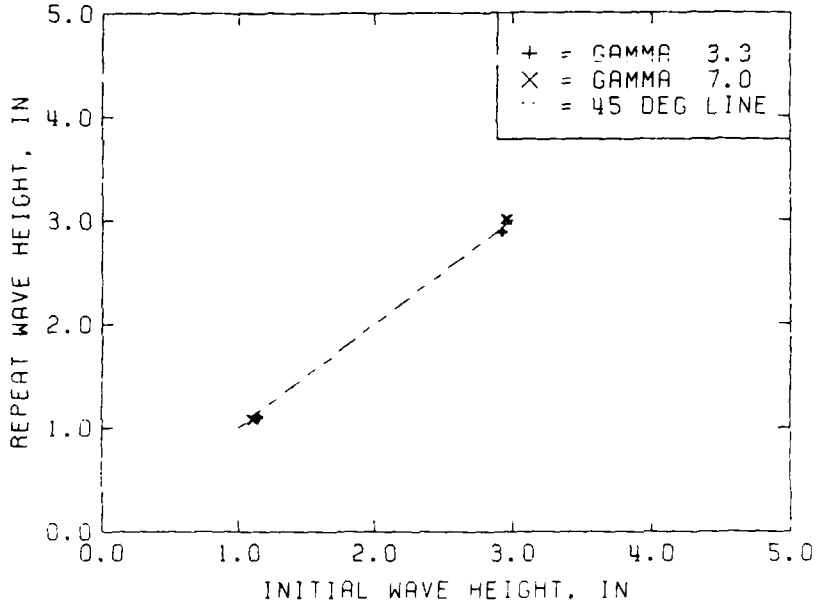

4 SPECTRAL CASES: CASES 1-4 VS. 27-30

Figure 12. Repeatability series of spectral wave heights

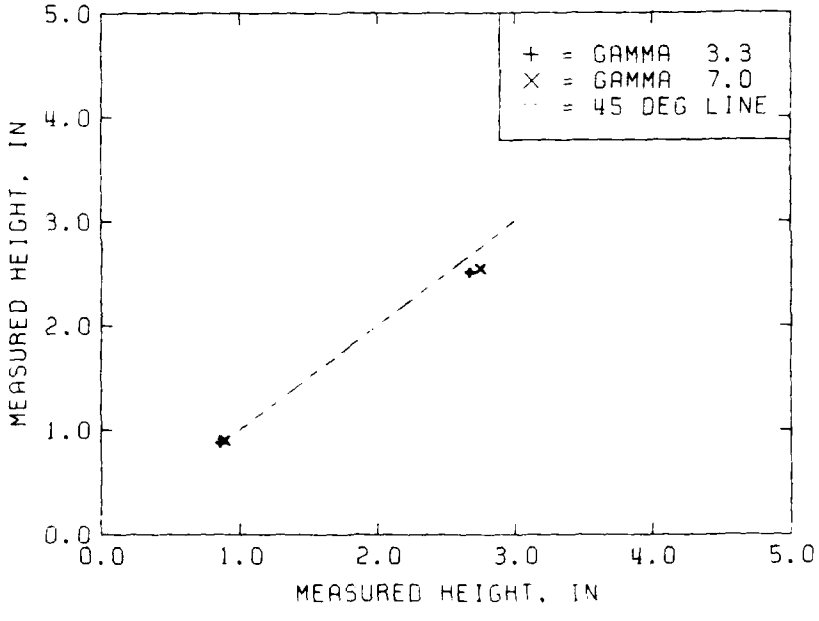

4 SPECTRAL CASES: CASES 13-16 VS. 31-34

Figure 13. Orientation series of spectral wave heights

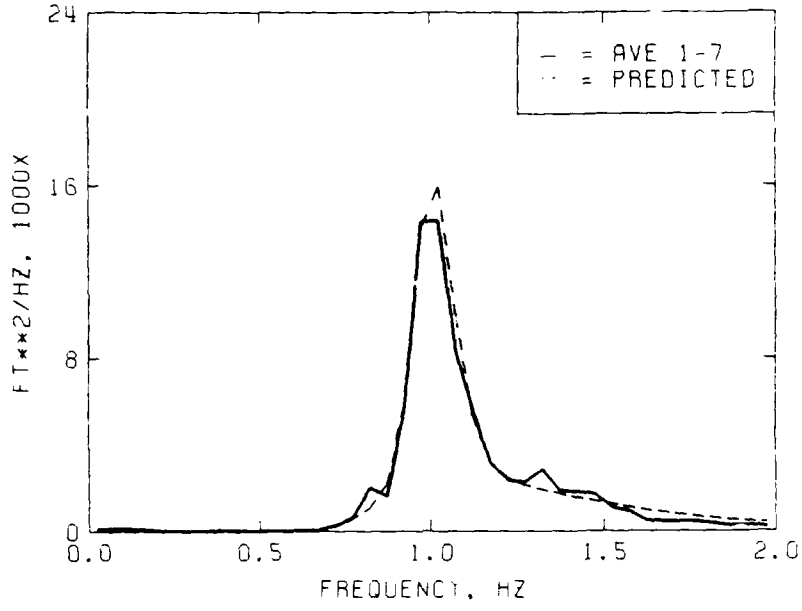

TP=1.00, HMO=3.00, G=7.0, D=0, SW=.05

Figure 14. Measured versus predicted frequency spectra

energy is relatively small. Any deviations from the predicted values can be the result of low SNR's (signal-to-noise ratio) or the presence of bounded or free long waves. The RAO's (see paragraph 93) indicated substantial differences which are hidden in the frequency spectra graphs because of the linear scale. The high frequency tail energy for all cases, however, was never more than two times greater than the predicted value. The largest variations occurred for an H_{m0} of 1 in. The RAO transfer functions should be able to correct for the observed differences in one or more iterations.

Unidirectional Spectral Analysis

88. Unidirectional spectral analysis results include peak frequency estimates, plots of directional spreading for all 34 cases at the peak frequency, and a comparison of the DSA and NSA methods of spectral simulation for two cases.

Peak frequency estimates

89. The measured peak frequencies agreed with the target values in all cases within ±0.01 Hz.

Directional spreading function

90. The measured-versus-predicted directional spreading function estimates for case 4 are shown in Figure 15. The spreading functions for the other 33 cases are included in Appendix E. The average of all seven gages is used for the measured results and of all 61 paddles for the predicted values. The truncation of the fourier series tends to produce negative side lobes as an artifact of the fourier transform method. Thus, negative spreading function estimates can sometimes be produced at wave directions on either side of the mean wave direction. These negative values have been suppressed and set to zero on these plots.

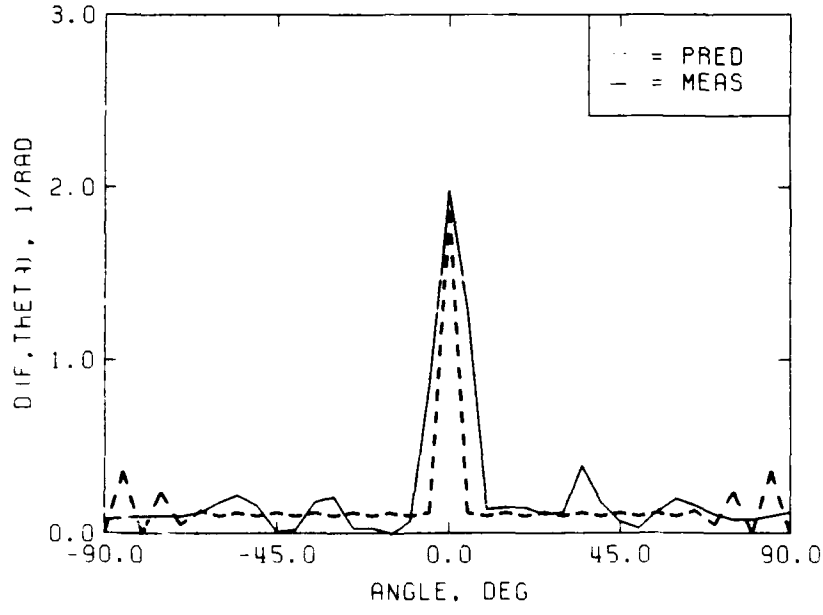

CASE 4: U12211, FP=1.00, HMO=3, G=7.0, D=0, S=1

Figure 15. Measured versus predicted directional spreading

91. These plots indicate the amount of directional spreading and the mean wave direction at the peak frequency. In all cases the measured value of mean wave direction agrees with the predicted values of 0, 30, or -30 deg. The agreement of the measured spreading with the predicted spreading is excellent for the cases with 1.0-sec peak period. The larger period cases indicate a wider spreading than predicted, which increases with increasing peak period. A possible explanation for the differences could be a frequency-dependent artifact of the simulation and analysis programs. A different random number

seed in the simulation program might produce a different realization with more stable characteristics. Also, the analysis program might be introducing artificial smoothing of the spreading estimates. MLM and Maximum Entropy Method (MEM) are analysis techniques which tend to give higher resolution. The measured data might be analyzed using both of these methods to determine if more stable results can be obtained. Another possible explanation of this difference in measured spreading may be the departure of the frequency spectra from the desired value. Since the directional wave spectrum is the product of the frequency spectra and the spreading function, any change in the frequency spectrum will cause a corresponding change in the spreading function. By increasing the spectral peak energy using the appropriate RAO, the spreading function may increase and become narrower.

DSA and NSA comparison

92. A comparison of the DSA and NSA amplitude methods for simulating unidirectional wave spectra was made for two cases. Target spectral parameters were T_p = 1.0 sec , H_{m0} = 2.0 in., γ = 7.0 , and θ_m = 0 deg. This case is similar to case 4 except that the wave height is smaller. It corresponds to a very narrow directional spectrum in both frequency and direction: conditions most necessitating use of the NSA method. Figures 16 and 17 show

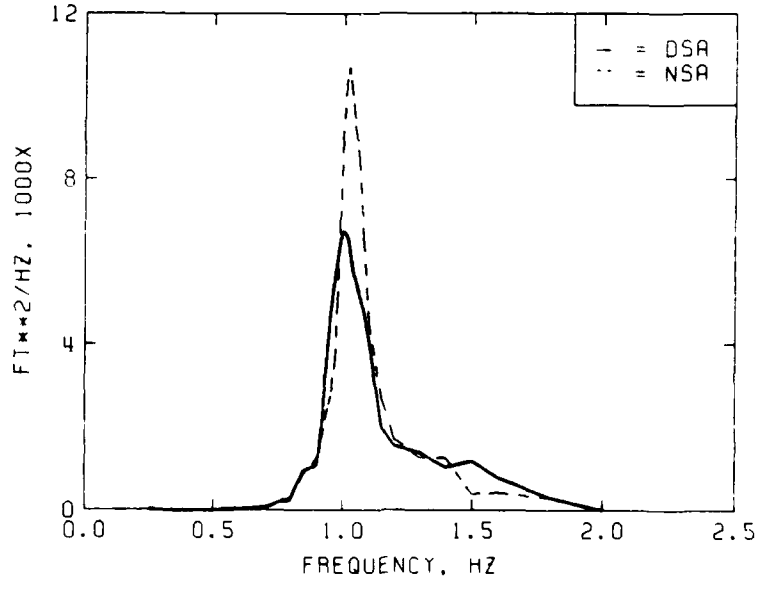

CASES 35 & 36: TP=1.0, HM0=2, G=7.0, D=0, S=1

Figure 16. Measured frequency spectra for DSA

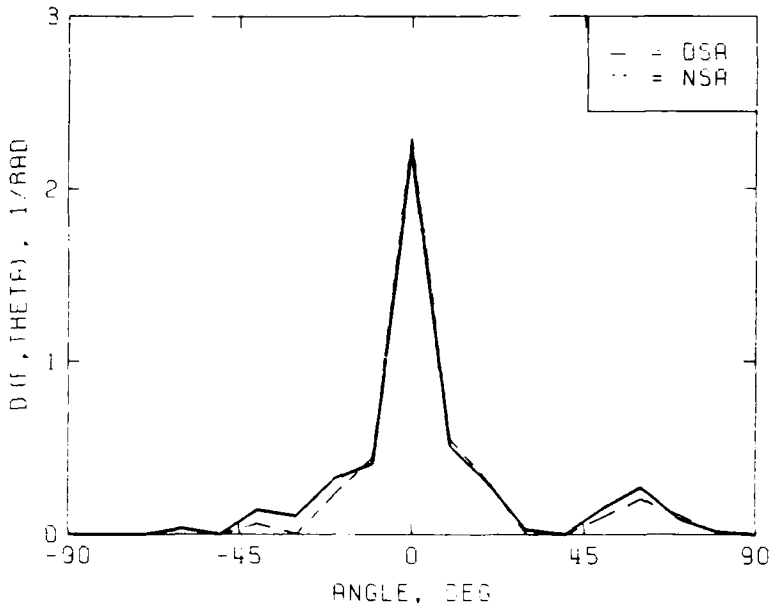

CASES 35 & 36: TP=1, HMO=2, G=7.0, D=0, S=1

Figure 17. Measured spreading functions for DSA and NSA methods

the measured frequency spectra and spreading functions, respectively, for both methods. Even though the frequency spectrum for the NSA method is larger than that for the DSA, the measured wave height for each was 2.04 and 2.16 in., respectively. Both values are statistically acceptable. The NSA value represents a larger realization within the realm of probability. The peak wave periods for both methods agree with the predicted value. Finally, the measured spreading functions show little variation with each other. Thus, the DSA method is a satisfactory method for simulating directional wave spectra in laboratory basins.

Response Amplitude Operator Functions

93. Figure 18 is a semilog plot of the RAO transfer function for case 4. The RAO's for the other cases are included in Appendix F. The RAO's for each gage and the average for all seven are shown. The RAO estimates were Gaussian smoothed to 0.05 Hz, and all estimates within contiguous 0.05-Hz bands were averaged. Values less than 1.0 indicate that the spectrum has to be increased at a particular frequency. Accordingly, values greater than 1.0

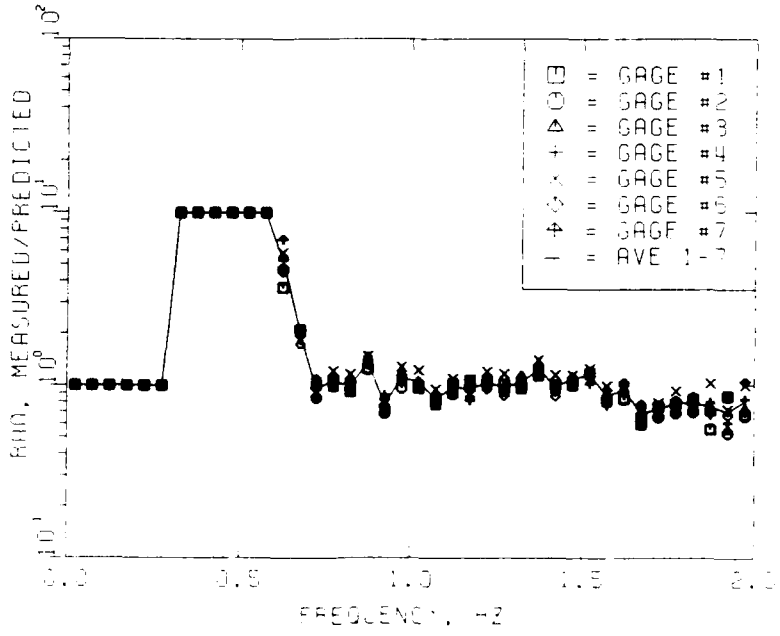

TP=1.00, HMO=3.00, G=7.0, D=0, BW=.05

Figure 18. RAO transfer function

indicate the opposite trend. As discussed previously, the RAO will be used in future tests to adjust the generated spectrum to compensate for DSWG and basin characteristics. This RAO correction will be especially helpful for the 1.5- and 2.0-sec peak period spectral cases.

Wave Grouping Analysis

94. In this section, comparisons between Goda's and Kimura's wave group analysis methods for a run of high waves are presented and discussed. The wave height time series plots from the zero-crossing analysis are presented first. Next, plots of correlation coefficients, probability distributions, mean run lengths, total run length, and Goda's peakedness parameter for both methods are presented.

Wave height time series

95. Figure 19 is a plot of the wave height time series for case 4. Appendix G contains plots for the other cases. The x-axis is individual zero-crossings or waves in a record instead of time. The y-axis is scaled with increments of 0.5 or 1.0 in. depending on the target wave height. Both mea-

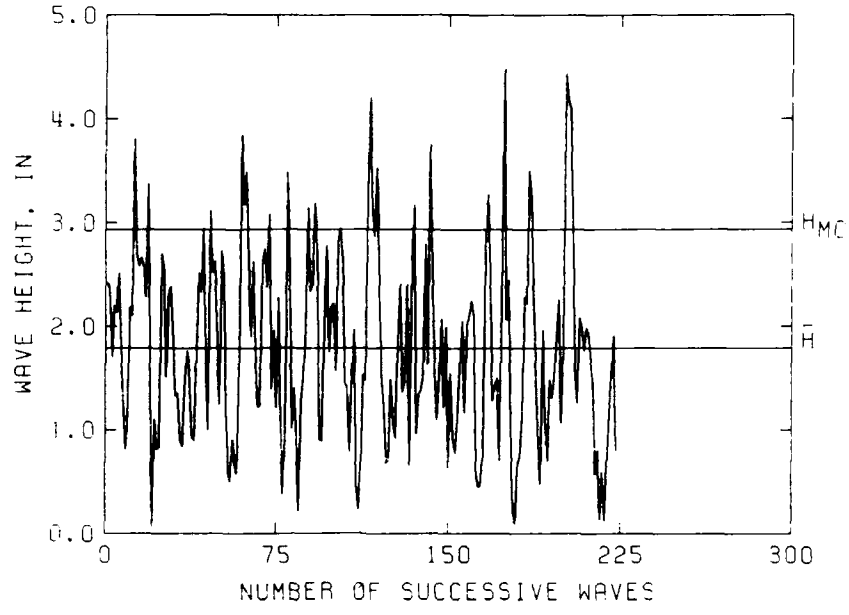

U12211, 3, FP=1.00, HMO=3.0, G=7.0, D=0, S=1, V=1
CHANNEL NUMBER = 7

Figure 19. Measured wave height time series

$\bar{H}$ (instead of H_m in these plots) and zero-moment H_{m0} wave height thresholds are shown. The measured number of crossings above these thresholds is used in the wave grouping analysis.

Correlation coefficients

96. Figures 20a to 20c show the effect of various lag lengths k between successive wave heights on $R_{hh}(k)$ for 0-deg cases with periods of 1.0, 1.5, and 2.0 sec, respectively. Each case is plotted separately in each figure. Figures 21a to 21c are analogous plots for the -30 deg cases. The $R_{hh}(k)$ for the 1.5- and 2.0-sec period cases at 0 deg may be artificially low because of the low directional spectra recorded. As expected, the correlation drops off rapidly for lags greater than one for all cases. The spectral cases with larger γ values have a higher $R_{hh}(k)$. Calculated values of $R_{hh}(1)$ for wind seas cases (i.e. γ = 3.3) generally agree with those of previous investigators (see paragraph 57). The cases for T_p = 1.0 sec are high, and those for T_p = 1.5 and 2.0 sec at 0 deg are low. For the swell cases (i.e. γ = 7.0 and 15.0), the agreement is good except for low values for T_p = 1.5 and 2.0-sec cases.

97. The $R_{hh}(k)$ for the 30-deg cases are uniformly higher than the

a. Peak period of 1.0 sec

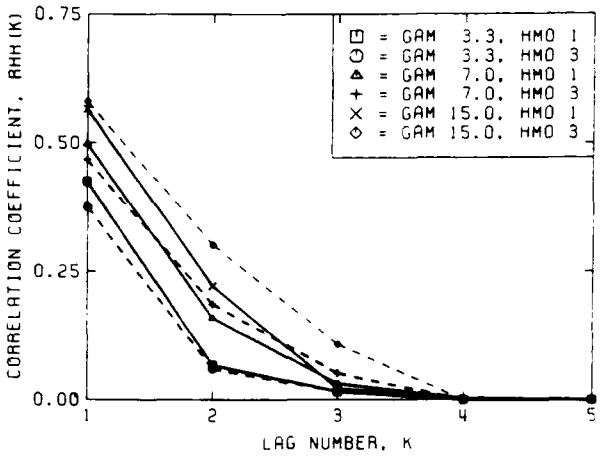

FOR TP = 1.0 SEC AND D = 0 DEG DATA

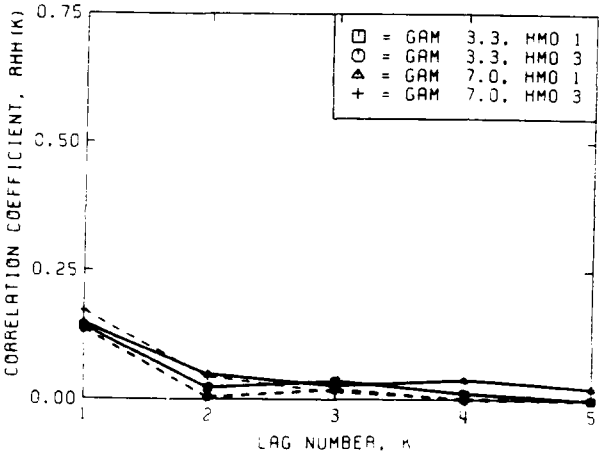

b. Peak period of 1.5 sec

FOR TP = 1.5 SEC AND D = 0 DEG DATA

c. Peak period of 2.0 sec

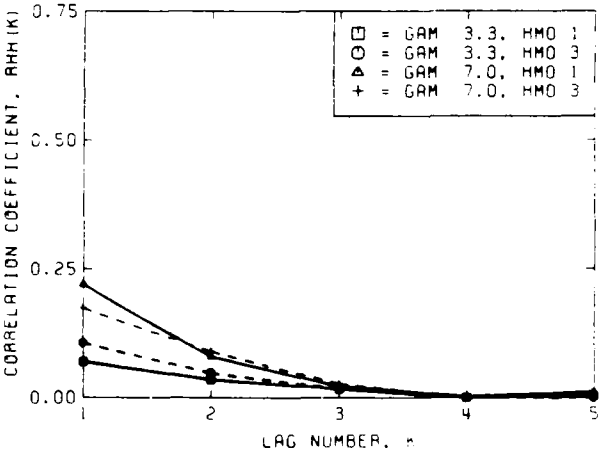

FOR TP = 2.0 SEC AND D = 0 DEG DATA

Figure 20. Effect of lag length on correlation coefficient at 0 deg

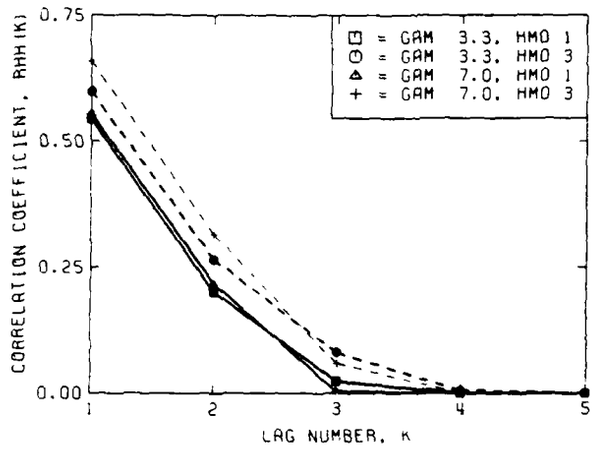

FOR TP = 1.0 SEC AND D = 30 DEG DATA

a. Peak period of 1.0 sec

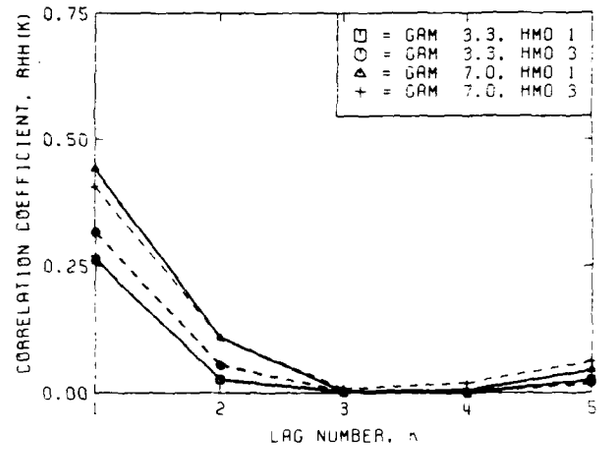

b. Peak period of 1.5 sec

FOR TP = 1.5 SEC AND D = 30 DEG DATA

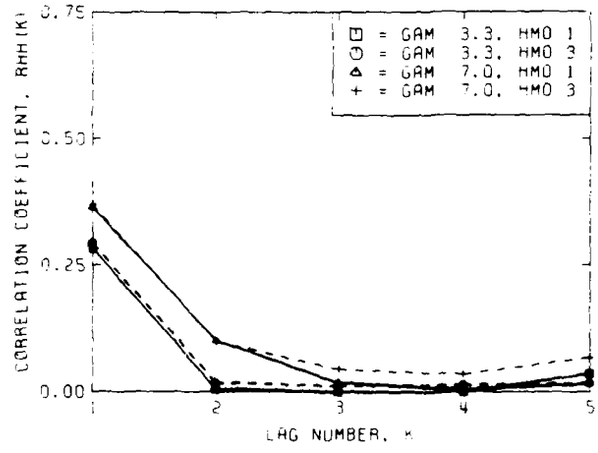

c. Peak period of 2.0 sec

FOR TP = 2.0 SEC AND D = 30 DEG DATA

Figure 21. Effect of lag length on correlation coefficient at 30 deg

corresponding 0-deg values. A cursory examination of the measured values for $R_{hh}(k)$ indicates a trigonometric relationship between 0- and 30-deg cases. Also, the T_p = 1.5- and 2.0-sec cases show an upturn in $R_{hh}(k)$ for lags greater than four indicating a correlation for every fifth wave. Further investigation into these relationships is warranted.

Probability distributions

98. Figures 22a and 22b show the probability for a run of high waves exceeding a specified run length for thresholds of H_m and H_{m0}, respectively, for case 4. The predicted Goda and Kimura probabilities are also plotted on each figure. The theoretical Goda line is a constant which only depends on the threshold value used. The theoretical Kimura line, however, is based on an average $R_{hh}(k)$ value for all lags, weighted mainly by $R_{hh}(1)$. A value of R_{hh} = 0.4 was used in Figures 22a and 22b. The calculated probabilities are predicted better by the Kimura model, regardless of threshold value.

99. The probability distributions for the other cases are contained in Appendix H. Values of R_{hh} of 0.2, 0.3, 0.4, 0.5, and 0.6 were used to calculate the theoretical Kimura probabilities based on the measured $R_{hh}(k)$ (see paragraphs 96 and 97). As expected (paragraph 49), the Goda model better predicted the broader spectra indicated by the lower $R_{hh}(k)$ values of 0.2.

Mean run length

100. Figures 23a and 23b show the relationship between the mean run length $\bar{j}_1$ for a threshold of H_m and the correlation coefficient $R_{hh}(1)$ for all 0- and 30-deg cases, respectively. Figures 24a and 24b show the corresponding relationship for a threshold of H_{m0}. The Goda and Kimura theoretical values are also shown in each figure. The measured values more closely match the Kimura predictions, although they are slightly lower. The difference between the two models is greater for the H_m threshold. Goda's model gives a constant value for different values of $R_{hh}(1)$ that seriously underpredicts the degree of wave grouping except for broad spectral cases with $R_{hh}(1) < 0.2$. These results are in agreement with those found by previous investigators (Goda 1983; Rye 1974; Kimura 1980; van Vledder 1983a,b; Elgar, Guza, and Seymour 1984; Thomas, Baba, and Harish 1986). The values of $R_{hh}(1)$ and j_1 are slightly higher for the 30-deg cases.

Total run length

101. Figures 25a and 25b illustrate the relationship between total run

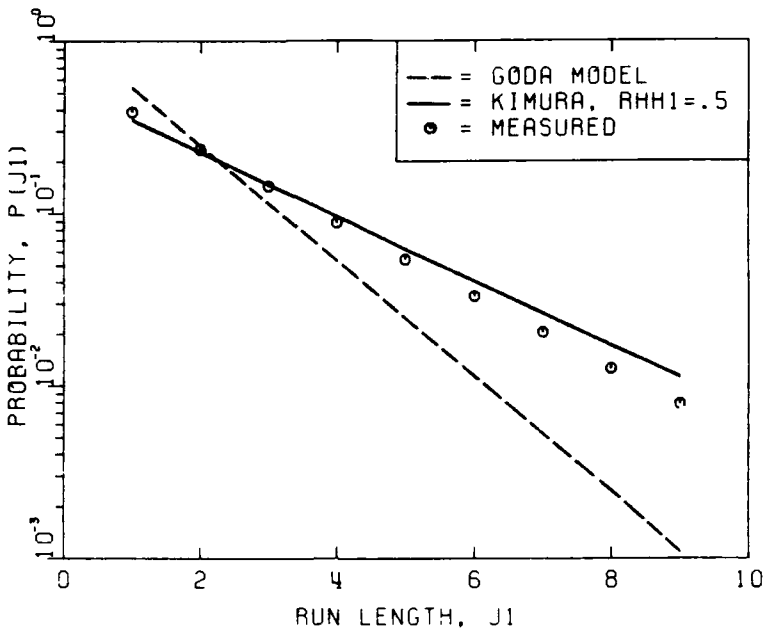

CASE 4: TP = 1.0, HMO = 3, G = 7.0, D = 0

a. Mean wave height threshold

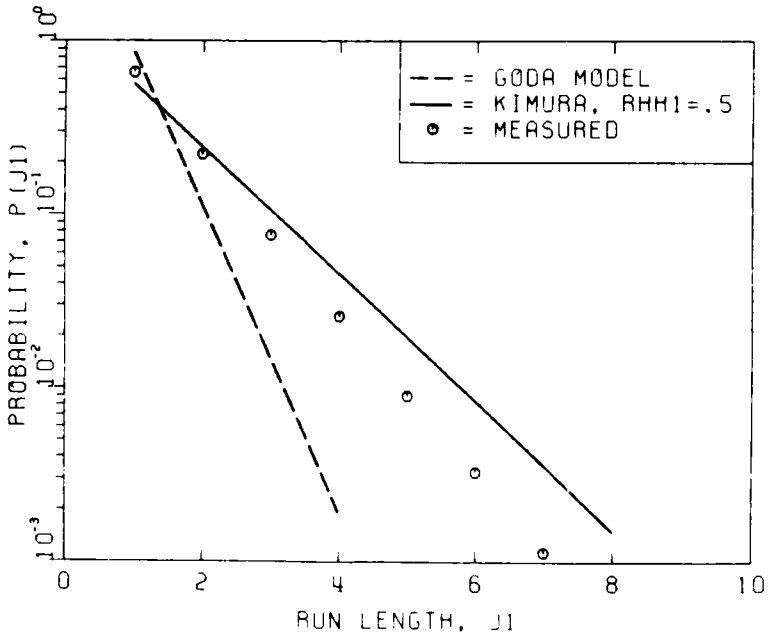

CASE 4: TP = 1.0, HMO = 3, G = 7.0, D = 0

b. Significant wave height threshold

Figure 22. Probability distribution for run of high waves

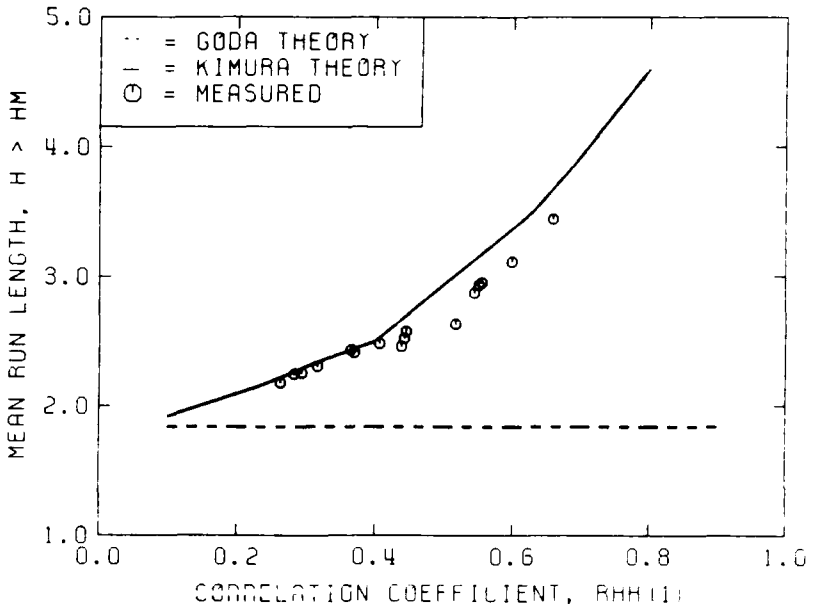

a. Cases of 0 deg

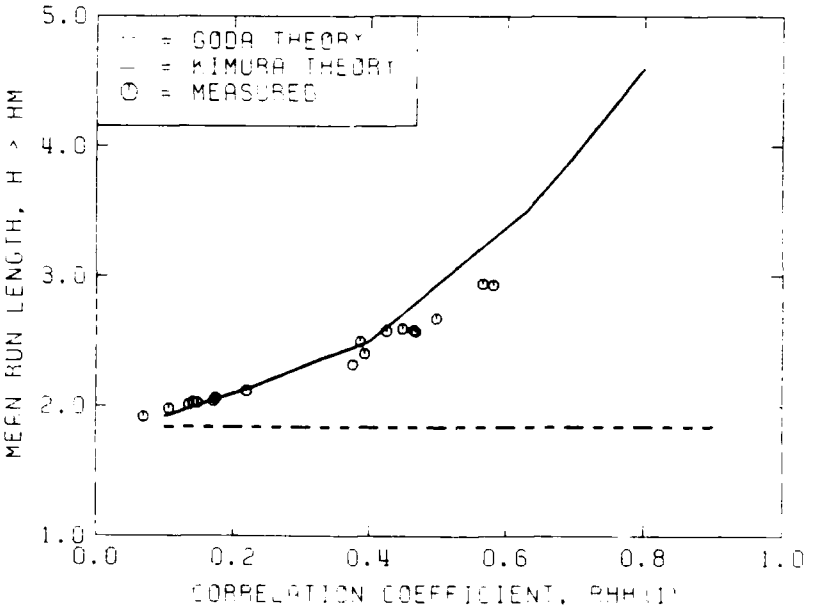

b. Cases of 30 deg

Figure 23. Run length versus correlation coefficient, mean height threshold

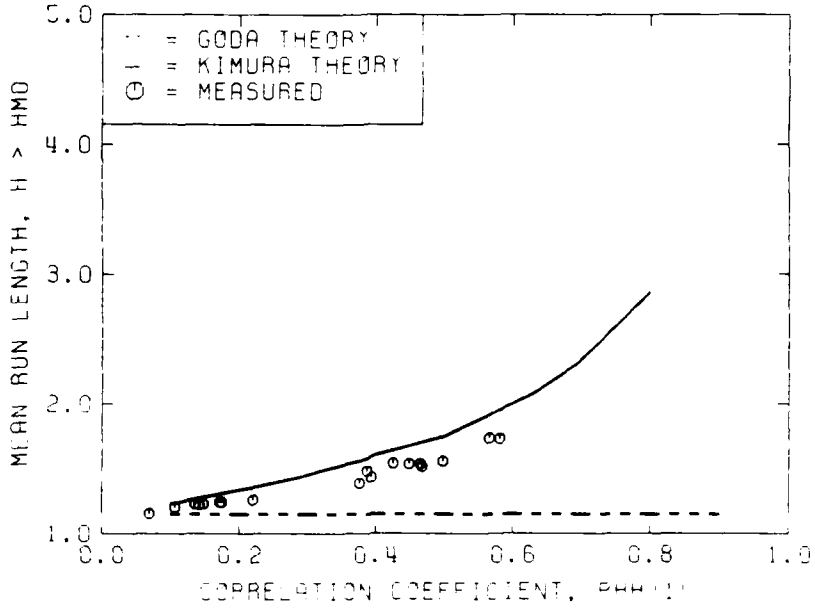

a. Cases of 0 deg

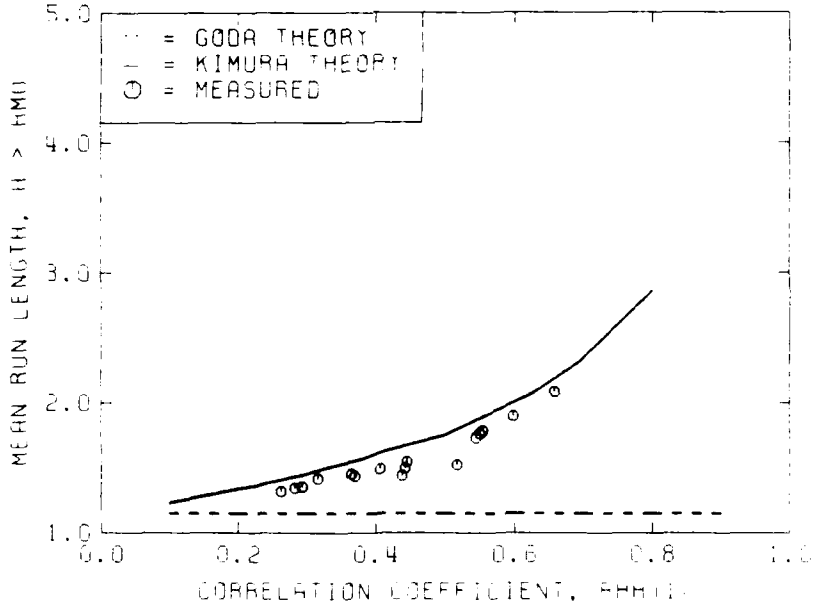

b. Cases of 30 deg

Figure 24. Run length versus correlation coefficient, significant height threshold

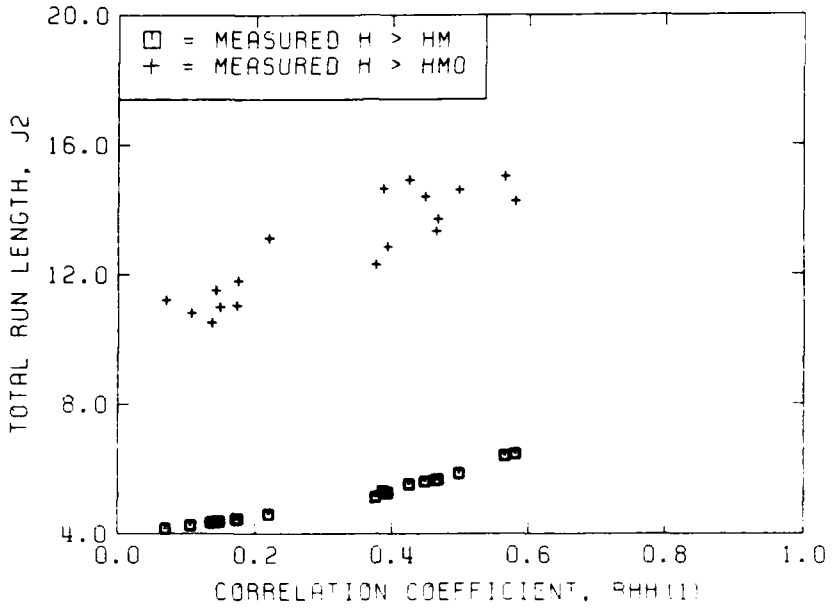

a. Cases of 0 deg

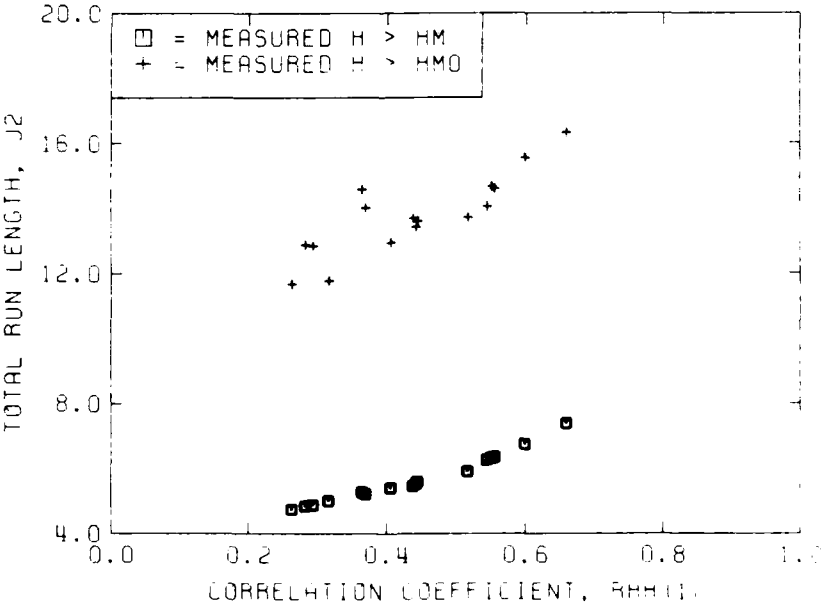

b. Cases of 30 deg

Figure 25. Total run length versus correlation coefficient

length j_2 and $R_{hh}(1)$ for the 0- and 30-deg cases, respectively. Values for both thresholds are shown in each figure. The data for the 30-deg cases substantiate the trends of the 0-deg cases. For a threshold of H_m, a strong linear or quadratic trend is indicated. For the H_{m0} threshold, the data show more scatter. A least squares fit could easily be calculated for both thresholds.

Goda's peakedness parameter

102. Goda (1970, 1976) proposed his spectral peakedness factor Q_p as a possible means of quantifying the degree of wave groupiness present. Its value ranges from 1 for white noise, 2 for wind waves, and 4-8 for swell conditions. Previous investigators (Yamaguchi 1981, Kimura 1980), in addition to Goda, found that the average group length increases as Q_p increases, and a narrow spectrum has a greater degree of grouping than a wide-banded spectrum. Long (1987), however, found that Q_p could have the same value for many different spectral shapes. Thus, although Q_p is probably not the best indicator of wave groupiness, it does show general trends.

103. Figures 26a and 26b illustrate the relationship between Kimura's predicted j_1 and Q_p for the 0- and 30-deg cases, respectively. Both threshold values are shown in each figure. The general trends for both thresholds are supported for both 0- and 30-deg cases. A strong linear or quadratic trend is evident in the 0-deg cases for both thresholds. There is more scatter for $Q_p > 4$ for the 30-deg cases, however. The data substantiates the trend toward an increase in $\overline{j_1}$ as Q_p increases.

104. Finally, $R_{hh}(1)$ is plotted as a function of Q_p for the 0- and 30-deg cases in Figures 27a and 27b, respectively. The solid line in each figure is the observed values of Goda (1976). The measured values agree with this data set. An increase in Q_p indicates an increase in $R_{hh}(1)$, with a possible leveling off or decrease at $Q_p > 5.5$.

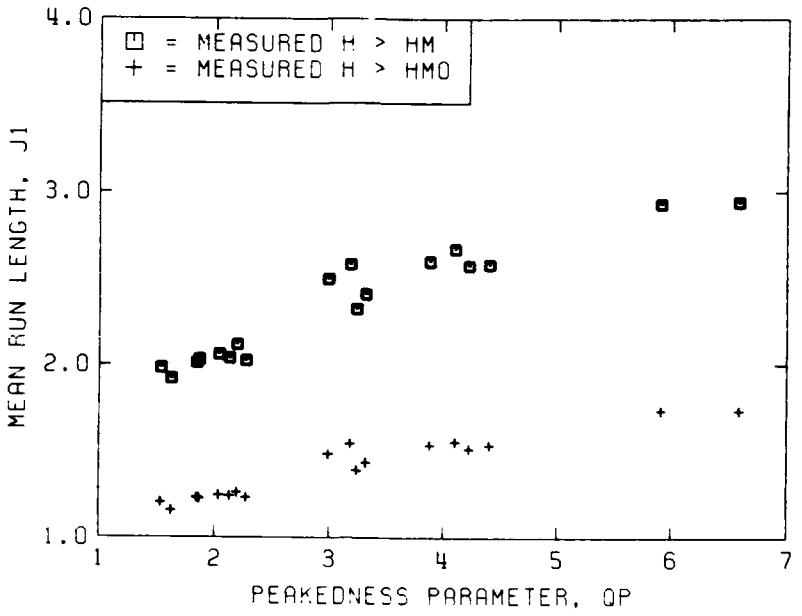

a. Cases of 0 deg

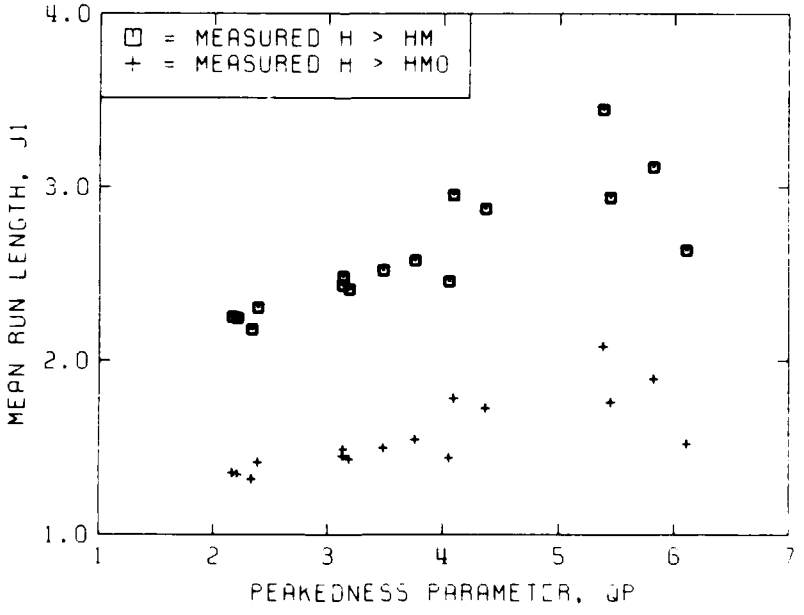

b. Cases of 30 deg

Figure 26. Mean run length versus Goda's peakedness parameter

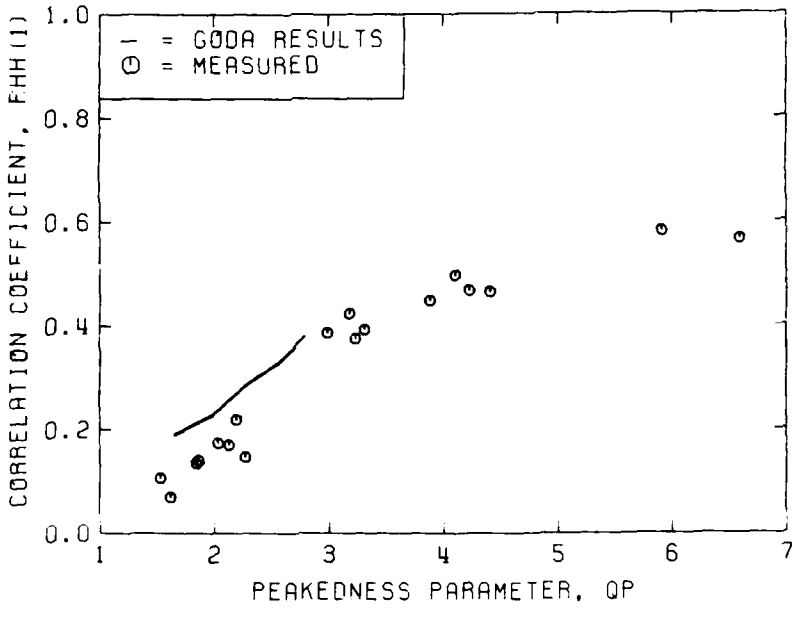

a. Cases of 0 deg

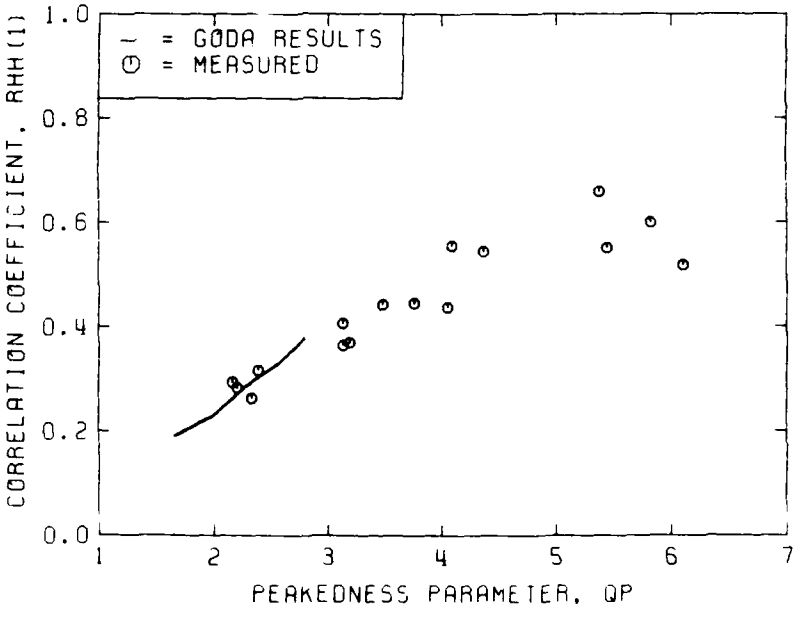

b. Cases of 30 deg

Figure 27. Correlation coefficient versus Goda's peakedness parameter

PART VI: SUMMARY AND RECOMMENDATIONS

105. The DSWG is an important resource for the study of naturally occurring sea conditions in laboratory physical models. Coastal structures respond differently to unidirectional spectral waves than they do to monochromatic waves. The modular design, portability, method of paddle connection and displacement, and electrical power of the DSWG produce clean, quiet unidirectional spectra from any peak direction without having to physically relocate the wave maker. Thus, transformation of wave energy in shallow and intermediate water depths due to shoaling, refraction, and diffraction can be more efficiently studied.

106. A series of 36 unidirectional spectral waves was generated to quantify performance characteristics of the DSWG basin. This report deals with the mechanics of simulating, generating, measuring, and analyzing unidirectional wave spectra. This assessment is a necessary first step in our overall research program to ensure accurate generation and analysis of naturally occurring waves prior to site-specific tests with coastal structures such as harbors, breakwaters, jetties, mounds, etc. The test series consisted of combinations of three wave periods, two zero-moment wave heights, three spectral peakedness parameters (narrowness of spectrum), and two peak wave directions covering a range of wave environments. Wave periods were 1.0, 1.5, and 2.0 sec; wave heights 1 and 3 in.; peakedness parameters 3.3, 7.0, and 15.0; and peak wave directions 0 and -30 deg. In addition, four tests were repeated to verify repeatability, and four tests were run at a peak direction of 30 deg to investigate the effect of wave orientation in the basin. Water depth for all tests was 1.0 ± 0.001 ft.

107. Measurements were made at seven locations within the basin by resistance and capacitance wave gages. Comparison of results between the two types of gages in a flume and in the basin indicated excellent agreement. The gages were arranged in a 2-3-1-7 linear array embedded in a directional array in the shape of a cross. It was centrally located 20 ft in front of the DSWG along its center line. A unit lag spacing of 1.33 ft was selected to optimize resolution while minimizing spatial aliasing.

108. Unidirectional spectra were simulated as the product of a unimodal TMA frequency spectrum and an empirically derived wrapped normal directional spreading function. A stroke time series for each paddle was simulated in the

frequency domain using a double summation, deterministic amplitude, random phase model. Another method, the non-deterministic, random phase model, produces an exact Gaussian realization, but at the cost of more variability and computer time. Two cases were generated to compare the two methods. Results showed little difference for the spectral characteristics simulated.

109. Unidirectional spectral analysis was based on the fourier series expansion of the directional spreading function. The measured surface data for each gage was zero-meaned, windowed, fourier transformed with a "235" FFT, and Gaussian smoothed in the frequency domain to obtain the cross-spectral matrix of autospectra and cross-spectra. This matrix is substituted into the parameterized spreading function to obtain a set of N_2 simultaneous, linear equations. A least squares fourier transform method for numerical integration is used to invert a matrix of independent variables to solve for the fourier coefficients of the spreading function. The technique for doing this is a linear, stepwise regression model.

110. Because of leakage around and under a "wetback" wave maker, electronic and mechanical losses, use of linear wave theory, and basin response characteristics, the measured spectra may not faithfully reproduce the target spectra. The height-to-stroke transfer function only compensates for an ideal wave maker. Thus, an RAO transfer function was calculated for each spectral control signal to compensate for observed variations in peak period, wave height, or spectral shape. The RAO is the ratio of measured-to-predicted spectral density for each gage at each frequency. A Gaussian smoothed, averaged RAO value will be used to correct the original stroke control signal in the frequency domain prior to generating the spectra again.

111. High waves in groups can produce more damage than isolated high waves. Wave grouping is important in the motions and resonances of moored vessels, harbor resonance, structure stability, and overtopping of shore protection structures. Thus, it is necessary to accurately calculate and predict wave group statistics. Both Goda's and Kimura's models were compared using measured wave height time series. Goda's model assumes that successive wave heights are independent, an appropriate assumption for broad-banded spectra. Kimura's model assumes mutual correlation or dependence of successive heights, a condition which is most often observed in nature.

112. A minimum of 200 waves at the peak period was collected with a sampling frequency of 10 Hz. Zero downcrossing, spectral, unidirectional

spectral, frequency response, and wave grouping analyses were performed for each case. Averages for all seven gages of wave period, height, direction, spectral shape, directional spreading, RAO transfer functions, and wave group statistics were calculated.

113. Measured values of zero-crossing wave period $T_{H1/3,d}$ and height $H_{1/3,d}$ were averaged and normalized by target values. The zero-crossing values were lower than their corresponding spectral analysis values. The normalized values of $T_{H1/3,d}$ ranged from a low of 0.64 to a high of 0.96. The 1.0-sec wave period cases agreed well with the target values. The 1.5- and 2.0-sec period cases at 0 deg were the lowest. Normalized values of $H_{1/3,d}$ ranged from a low of 0.60 to a high of 1.07. Wave height decreased with increasing wave direction and period.

114. For spectral analysis, the data were zero-meaned, windowed, fourier transformed, and band averaged between lower and upper cutoff frequencies for 20 degrees of freedom. The measured spectral analysis peak period T_p and zero-moment wave height H_{m0} were also averaged and normalized by target values. The agreement between measured and target T_p was excellent. Normalized T_p ranged between 0.94 to 1.02. The normalized H_{m0} ranged from a low of 0.64 to a high of 1.15. Although the variation was less than the zero-crossing values, the values were lower than desired for the longer period cases at 0 deg.

115. The shape of the measured frequency spectra showed excellent agreement with the predicted values for the 1.0-sec cases regardless of wave height, direction, or spectral peakedness. The measured shapes for the longer period cases did not agree as well. The spectral peaks were usually smaller than the predicted values by a factor of the order of 2. This explains the low values for the H_{m0} heights. Low and high frequency tails were reasonably well predicted. The RAO transfer functions will be used prior to future runs to compensate for these observed differences in period, height, and shape.

116. The calculated peak periods and mean wave directions from the unidirectional spectral analysis agreed very well with target values. Excellent agreement was reached between the measured and predicted directional spreading estimates for the 1.0-sec cases. The longer period cases indicated a wider spread than predicted which increases with increasing period. Part of this departure may be explained by a frequency dependence of the simulation

and analysis software due to random number seeds, truncation of the fourier series, and sparsity of gages. Analysis of these cases with an MLM or MEM should give higher resolution and narrower spreading function estimates. Another source of error could be the smaller than desired frequency spectra at the peak period. All potential sources of error should be investigated further.

117. Wave group statistics calculated include correlation coefficients, probability distributions, mean and total run lengths, and correlations with Goda's peakedness parameter. The calculated correlation coefficients $R_{hh}(k)$ generally agreed with previously observed values, except for the low 1.5- and 2.0-sec cases at 0 deg. As expected, correlation drops off rapidly for lags greater than one and increases as the spectral peakedness (i.e. narrowness) of the spectra increases. The 30-deg cases had uniformly higher values than the corresponding 0-deg cases, indicating that a trigonometric relationship probably exists. A correlation for every fifth wave height was indicated for the 1.5- and 2.0-sec cases. These trends should be investigated further if possible.

118. For the H_m threshold, the Kimura model better matches the observed probabilities. For the H_{m0} threshold, the match is not as good but still better than that for the Goda model. As expected, the Goda model better predicted the broader spectral cases with $R_{hh}(1)$ less than 0.2.

119. Mean run lengths j_1 predicted by the Kimura method are slightly higher than measured values. Goda's model predicts a constant value which seriously underpredicts all cases except for broad spectral cases with $R_{hh}(1) > 0.2$. The 30-deg cases had slightly higher values than the corresponding 0-deg cases.

120. Total run lengths show a strong trend for both thresholds for both 0- and 30-deg cases. The H_m threshold trends show less scatter than the H_{m0} threshold values. A least squares fit could easily be calculated for both thresholds.

121. Although Goda's spectral peakedness parameter Q_p is probably not the best indicator of wave groupiness, it does show general trends. Increases in Q_p are observed with increases in $\overline{j_1}$ and $R_{hh}(1)$. A strong trend is evident in the 0-deg cases for both thresholds. For the 30-deg cases, more scatter is present for $Q_p > 4$. Finally, $R_{hh}(1)$ appears to level off for $Q_p > 5.5$.

REFERENCES

Abramowitz, M., and Stegun, I. A. 1970. Handbook of Mathematical Functions with Formulas, Graphs, and Mathematical Tables, Dover Publications, New York.

Arhan, M., and Ezraty, R. 1978. "Statistical Relations Between Successive Wave Heights," Oceanologica Acta, Vol 1, No. 2.

Battjes, J. A. 1974. "Computation of Set-up, Longshore Currents, Run-up and Overtopping due to Wind-Generated Waves," Thesis, Delft, The Netherlands.

Biesel, F. 1954. "Wave Machines," Proceedings of the 1st Conference on Ships and Waves, Hoboken, NJ, pp 288-304.

Borgman, L. E. 1969 (May). "Directional Spectra Models for Design Use," OTC 1069, Offshore Technology Conference, Houston, TX.

_____. 1979. "Directional Wave Spectra from Wave Sensors," Ocean Wave Climate, M. Earle and A. Malahoff, eds., Plenum Press, New York, pp 269-300.

_____. 1984 (Nov). "Directional Spectrum Estimation for the Sxy Gauges," Report to US Army Engineer Waterways Experiment Station, L. E. Borgman, Inc., pp 1-104.

Borgman, L. E., and Panicker N. N. 1970. "Design Study for a Suggested Wave Gage Array off Point Mugu, California," Hydraulic Engineering Laboratory, University of California at Berkeley, Technical Report HEL 1-14, pp 1-23.

Briggs, M. J. 1987a. "Wave Group Analysis Based on Kimura's Method," Technical Report CERC-87-14, US Army Engineer Waterways Experiment Station, Vicksburg, MS.

_____. 1987b. "Analysis of Wave Grouping in a Laboratory Basin Using Kimura's Method," IAHR Seminar on Wave Analysis and Generation in Laboratory Basins, Lausanne, Switzerland, pp 285-302.

_____. 1987c. "Generation of Directional Spectral Waves in Shallow-Water Basins," Presented at IAHR 22nd Congress, Lausanne, Switzerland, pp 1-6.

Briggs, M. J., and Barnes, L. (Submitted). "Passive Wave Absorber Design for Laboratory Basins," Journal of Waterway, Port, Coastal and Ocean Engineering, American Society of Civil Engineers.

Briggs, M. J., and Hampton, M. L. 1987. "Directional Spectral Wave Generator Basin Response to Monochromatic Waves," Technical Report CERC-87-6, US Army Engineer Waterways Experiment Station, Vicksburg, MS.

Briggs, M. J., Borgman, L. E., and Outlaw, D. G. 1987. "Generation and Analysis of Directional Spectral Waves in a Laboratory Basin," OTC 5416, Offshore Technology Conference, Houston, TX, pp 495-502.

Elgar, S., Guza, R. T., and Seymour, R. J. 1984. "Groups of Waves in Shallow Water," Journal of Geophysical Research, Vol 89, No. C3, pp 3623-3634.

_____. 1985. "Wave Group Statisitics from Numerical Simulations of a Random Sea," Applied Ocean Research, Vol 7, No. 2, pp 93-96.

Goda Y. 1970. "Numerical Experiments on Wave Statistics with Spectral Simulation," Report of Port and Harbour Research Institute, Vol 9, No. 3, pp 3-57.

_____. 1976. "On Wave Groups," Proceedings, BOSS '76 Conference, Trondheim, Norway.

_____. 1983 (Mar). "Analysis of Wave Grouping and Spectra of Long-Traveled Swell," Report of Port and Harbour Research Institute.

_____. 1985. Random Seas and Design of Maritime Structures, University of Tokyo Press, Japan.

Hudspeth, R. T., Nath, J. H., and Sollitt, C. K. 1983. "Digital to Analog Wavemaker Simulations," Symposium on Physical Modeling in Coastal Engineering, University of Delaware, Newark, DE, pp 81-103.

International Association of Hydraulic Research Working Group on Wave Generation and Analysis. 1986 (Jan). "List of Sea State Parameters," Supplement to Bulletin No. 52, pp 1-24.

Isaacson, M. 1985. "Laboratory Measurement and Generation of Directional Surface Waves," Presented at IAHR 21st Congress, Melbourne, Australia.

Jennrich, R. I. 1977. "Stepwise Regression," in Statistical Methods for Computers, K. Enslein, A. Ralston, and H. Wilf, eds., Wiley InterScience, pp 58-75.

Kimura, A. 1980. "Statistical Properties of Random Wave Groups," Proceedings of the 17th International Conference on Coastal Engineering, pp 2955-2973.

Kitaigorodskii, S. A. et al. 1975. "On Phillops Theory of Equilibrium Range in the Spectra of Wind Generated Gravity Waves," Journal of Physical Oceanography, Vol 5, pp 410-420.

Long, C. E. "Laboratory Wave Generation and Analysis: An Instructional Report for Unidirectional Wave Generation and Analysis" (in preparation), US Army Engineer Waterways Experiment Station, Vicksburg, MS, pp 1-32.

_____. 1987. "Some Comments on Goda's Peakedness Parameter," American Society of Civil Engineers Specialty Conference on Coastal Hydrodynamics, University of Delaware, Newark, DE, pp 32-45.

Outlaw, D. G., and Briggs, M. J. 1986 (Aug). "Directional Irregular Wave Generator for Shallow Water Basins," 21st American Towing Tank Conference, Washington, DC, pp 1-6.

Pinkster, J. A. 1984. "Numerical Modelling of Directional Seas," Proceedings, Symposium on Description and Modelling of Directional Seas, Technical University of Denmark, Copenhagen.

Rice, S. O. 1944. "Mathematical Analysis of Random Noise," Reprinted in Selected Papers on Noise and Stochastic Processes, Dover Publications, Inc., New York.

_____. 1945. "Mathematical Analysis of Random Noise," Bell System Technical Journal, Vol 24.

Rye, H. 1974. "Wave Group Formation among Storm Waves," Proceedings of the 14th International Conference on Coastal Engineering, Vol 1, pp 1964-1983.

Sand, S. E. 1979. "Three-Dimensional Structure of Ocean Waves," Series Paper No. 24, Institute of Hydrodynamics and Hydraulic Engineering, Technical University of Denmark, Sweden.

Sand, S. E., and Mynett, A. E. 1987. "Directional Wave Generation and Analysis," IAHR Seminar Maritime Hydraulics Section, XXII Congress, Lausanne, Switzerland, pp 209-235.

Searle, S. R. 1982. Matrix Algebra Useful In Statistics, John Wiley and Sons, New York.

Thomas, K. V., Baba, M., and Harish, C. M. 1986 (Jul). "Wave Groupincss in Long-Traveled Swell," Journal of Waterway, Port, Coastal and Ocean Engineering, American Society of Civil Engineers, Vol 112, No. 4, pp 498-511.

Tucker, M. J., Challenor, P. G., and Carter, D. J. T. 1984. "Numerical Simulation of a Random Sea: A Common Error and its Effect upon Wave Group Statistics."

Van Vledder, G. Ph. 1983a. "Preliminary Investigation into the Characteristics of Wave Groups in Sea States and Swell," Delft Technical University, Graduate Thesis, 1st of 3 Parts, pp 1-66.

_____. 1983b. "Testing of the Kimura Model for the Description of Wave Groups," Delft Technical University, Graduate Thesis, 2nd of 3 Parts, pp 1-119.

Vincent, C. L. 1984 (Sep). "Shallow Water Waves: A Spectral Approach," Proceedings of the 19th International Conference on Coastal Engineering, Houston, TX, pp 370-382.

Yamaguchi, M. 1981. "Statistical Properties of Wind Waves in Limited Fetch," Memoirs of the Ehime University, Sec. III, Vol IX, No. 4.

APPENDIX A: NOTATION

a_j	Real fourier coefficient of spreading function
$A(f)$	Deterministic spectral amplitude
b	Resolution bandwidth
b_j	Imaginary fourier coefficient of spreading function
$\{B\}$	Regression coefficients vector
B_{ij}	Dummy variable for directional spectra
$C_{ij}(f)$	Cospectral density estimate
$D(f,\theta)$	Directional spreading function
$\{DIR\}$	Vector of directional fourier coefficients, frequency f
f	Frequency
f_ℓ	Lower cutoff frequency
f_p	Spectral peak frequency
f_u	Upper cutoff frequency
$F_3(f,\theta)$	Three-dimensional wave height transfer function
g	Gravitational constant
h	Water depth
H	Wave height
H_b	Maximum prebreaking wave height at wave maker
H_c	Cutoff or threshold wave height
H_m	Mean wave height
H_{m0}	Zero-moment wave height
$H_{1/3,d}$	Zero downcrossing significant wave height
i	Imaginary unit number
j	Summation index
j_1	Mean run length index
$\overline{j_1}$	Mean run length for run of high waves
j_2	Total run length index
$\overline{j_2}$	Mean run length for total run
k	Wave number
kh	Nondimensional water depth
k_m	Wave number at frequency $m\Delta f$
k_y	Y-axis component of wave number
K	Integer exponent for factor 2 in "235" FFT
ℓ	Space domain summation index

L	Linear, shallow-water wavelength Number of harmonics in directional spreading function Integer exponent for factor 3 in "235" FFT
L_p	Wavelength associated with peak frequency f_p
L_y	Y-axis component of wavelength
m	Frequency domain summation index
m_0	Zero moment
M	Equivalent number of bands for Gaussian smoothing Integer exponent for factor 5 in "235" FFT
n	Time domain summation index
N	Total number of data samples Number of harmonics in Fourier series Number of wave gages Number of zero crossings in wave height time series
p	Probability wave height $\geq$ threshold wave height
$[p]$	Transition probability matrix
$P(j_1)$	Probability of run length having length of j_1
$P(x)$	Normal probability function
P_{11}	Probability neither successive wave exceeds threshold
P_{22}	Probability of simultaneous exceedance both heights
q	Probability wave height $<$ threshold wave height
Q_p	Goda's spectral peakedness parameter
$Q_{ij}(f)$	Quadrature spectral density component
RAO_i	Response amplitude operator function for Gage i
$R_{hh}(k)$	Correlation coefficient for every k^{th} wave
$R_{hh}(1)$	Correlation coefficient for successive waves
s_c	Stroke control signal
$S(f)$	Frequency spectrum
$\bar{S}(f)$	Harmonic mean of autospectral density estimate
$\bar{S}_m$	Gaussian smoothed spectral density at frequency $m\Delta f$
$S(f,\theta)$	Directional wave spectrum
$S_{ii}(f)$	Autospectral density estimate
$S_{ij}(f)$	Cross-spectral density estimate
$S_J(f)$	JONSWAP frequency spectrum
$S_p(f)$	Predicted frequency spectrum
$S_{TMA}(f)$	TMA frequency spectrum
{SPECTRA}	Vector of measured autospectra and cross-spectra, frequency f
t	Time

T	Wave period
$T_{H1/3,d}$	Zero downcrossing significant period
T_p	Spectral peak period
T_r	Length of time series
[TRANSFER]	Matrix of directional spectra terms at frequency f
$U(f)$	Real amplitude component of A(f)
U_m	Real fourier coefficient of control signal at $m\Delta f$
$V(f)$	Imaginary amplitude component of A(f)
V_m	Imaginary fourier coefficient of control signal at $m\Delta f$
w_j	Weighting function for Gaussian smoothing
x	X-axis coordinate Random variable
[X]	Matrix of independent variables in regression analysis
X_{ij}	Distance between Gages i and j along x-axis
y	Y-axis coordinate
{Y}	Dependent variables vector in regression analysis
Y_{ij}	Distance between Gages i and j along y-axis
α	Spectral parameter
γ	Peak enhancement factor
Δf	Basic frequency increment
Δt	Time interval
ϵ	Wave steepness
$\{\epsilon\}$	Prediction errors vector
$\eta(x,y,t)$	Water surface elevation time series
θ	Wave direction, angle of wave propagation
θ_m	Principal or mean wave direction at frequency $m\Delta f$
θ_0	Constant term of θ_m
θ_1	Slope term of θ_m
$\bar{\theta}$	Overall mean wave direction for all frequencies
κ	Correlation parameter
π	3.14159
σ	Directional spreading standard deviation
σ_a	Left spectral width parameter
σ_b	Right spectral width parameter
σ_m	Mean spreading standard deviation
σ_0	Constant term of σ_m

σ_1	Slope term of σ_m
ϕ	Directional spectra dummy variable
Φ	Finite depth spectral factor Independent, random phase
Ω_h	TMA finite-depth parameter